ELSEVIER

Chemical Geology 227 (2006) 1–25

CHEMICAL GEOLOGY
INCLUDING
ISOTOPE GEOSCIENCE

www.elsevier.com/locate/chemgeo

Partitioning of Ni, Co and V between spinel-structured oxides and silicate melts: Importance of spinel composition

K. Righter [a,*], W.P. Leeman [b], R.L. Hervig [c]

[a] *Mailcode KT, NASA Johnson Space Center, 2101 NASA Pkwy., Houston, TX, USA*
[b] *Department of Earth Sciences, Rice University, Houston, TX 77251-1892, USA*
[c] *Center for Solid State Science, Arizona State University, Tempe, AZ 85287, USA*

Received 8 July 2004; received in revised form 5 May 2005; accepted 30 May 2005

Abstract

Partitioning of Ni, Co and V between Cr-rich spinels and basaltic melt has been studied experimentally between 1150 and 1325 °C, and at controlled oxygen fugacity from the Co-CoO buffer to slightly above the hematite–magnetite buffer. These new results, together with new Ni, Co and V analyses of experimental run products from Leeman [Leeman, W.P., 1974. Experimental determination of the partitioning of divalent cations between olivine and basaltic liquid, Pt. II. PhD thesis, Univ. Oregon, 231–337.], show that experimentally determined spinel–melt partition coefficients (D) are dependent upon temperature (T), oxygen fugacity (fO_2) and spinel composition. In particular, partition coefficients determined on doped systems are higher than those in natural (undoped) systems, perhaps due to changing activity coefficients over the composition range defined by the experimental data. Using our new results and published runs ($n=85$), we obtain a multilinear regression equation that predicts experimental D(V) values as a function of T, fO_2, concentration of V in melt and spinel composition. This equation allows prediction of D(V) spinel/melt values for natural mafic liquids at relevant crystallization conditions. Similarly, D(Ni) and D(Co) values can be inferred from our experiments at redox conditions approaching the QFM buffer, temperatures of 1150 to 1250 °C and spinel composition (early Cr-bearing and later Ti-magnetite) appropriate for basic magma differentiation. When coupled with major element modelling of liquid lines of descent, these values (D(Ni) sp/melt=10 and D(Co) sp/melt=5) closely reproduce the compositional variation observed in komatiite, mid-ocean ridge basalt (MORB), ocean island basalt (OIB) and basalt to rhyolite suites.
Published by Elsevier B.V.

Keywords: Trace element partitioning; Spinel; Fractional crystallization; Chromite; Magnetite

1. Introduction

Spinel-structured oxides are known to concentrate certain transition metals and thus play an important role in controlling, for example, Ni, Co, Cr and V contents in basic and ultrabasic magmas during differentiation (e.g., Irving, 1978). Extensive solid solution between aluminous-, chromian-, titanian- and ferric iron-bearing end members makes the compositions of these oxide minerals in natural systems quite variable. Previous studies have shown extremely compatible behavior for Ni and Co, indicating partition coefficients D(M) (defined as weight of an element M in the mineral phase divided by the weight of M in the co-existing melt) as high as 70 for D(Ni) and 15 for D(Co) in magnetite (e.g., Nielsen et al., 1994). Available experimental data indicate that D(M) values for spinel are strongly dependent upon variables such as temperature (T), composition and oxygen fugacity (fO_2). For in-

* Corresponding author.
E-mail address: kevin.righter-1@nasa.gov (K. Righter).

0009-2541/$ - see front matter. Published by Elsevier B.V.
doi:10.1016/j.chemgeo.2005.05.011

Table 1
Starting compositions used in this study

	1	2	3
	Ankaramite	*KI-22*	*70-15*
SiO_2	43.66	45.93	47.1
TiO_2	2.97	2.03	3.03
Al_2O_3	13.13	9.62	15.2
FeO*	14.84	12.75	13.44
MnO	0.21	0.18	0.18
MgO	9.75	18.95	7.58
CaO	12.12	8.86	9.50
Na_2O	2.5	1.63	2.59
K_2O	0.86	0.38	0.74
P_2O_5	0.37	0.19	0.50
Total	101.15	100.52	99.86

(1) Hawaiian ankaramite (Chen et al., 1990).
(2) Kilauea Iki picrite (Leeman, 1974).
(3) Snake River Plain olivine tholeiite (Leeman, 1974).

stance, chromite stability is temperature- and oxygen fugacity-dependent (Barnes, 1986; Roeder and Reynolds, 1991; Hanson and Jones, 1998), and partitioning of V between magnetite and melt is fO_2-dependent due to the variable valence of V—between 3+ and 5+ (Lindstrom, 1976). Despite this knowledge, a comprehensive understanding of Ni, Co and V partitioning remains elusive. Nielsen et al. (1994) attempted to quantify the T, fO_2 and spinel compositional dependence of D(V), but was unable to satisfactorily reproduce the available data. We have tried similar approaches to parameterize D(Ni) and D(Co) with no greater success. Such efforts clearly show that the currently available data sets are inadequate to constrain the systematics of compatible trace element partitioning between spinel and silicate melt.

To better understand Ni, Co and V partitioning during basic magma differentiation, we carried out four series of experiments designed to generate spinels with a large compositional range such as in natural systems with Ti–Al–Cr–Fe. In addition, we analyzed the experiments of Leeman (1974) on natural basalts—in some cases doped with up to 2% of Ni and Co, but with natural concentrations of other elements. Together with previous experiments, these new measurements reveal a large difference in partition coefficients derived from doped and undoped experiments; partition coefficients determined from undoped experiments are as much as a factor of 10 lower than those from previous work on doped systems. In addition, we demonstrate the importance of spinel compositional variation on partition coefficients, especially for V.

2. Experimental techniques

A Hawaiian ankaramite, doped with 1% of Cr_2O_3 in order to ensure the stability of spinel as demonstrated previously by Roeder and Reynolds (1991), was used to study spinel–melt equilibrium (Table 1). This composition was placed in 3 mm o.d. $Au_{75}Pd_{25}$ capsules (0.15 mm walls) and crimped (but not welded) at the top to allow equilibration of the sample with the buffer. These capsules were then placed in an evacuated silica tube with an alumina crucible containing various oxy-

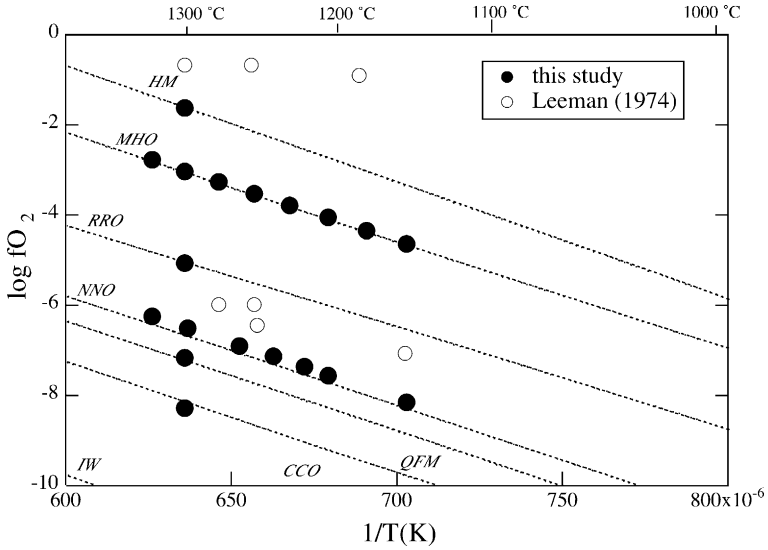

Fig. 1. Summary of temperature vs. fO_2 for the experiments reported in this study and those from Leeman (1974). Buffer curves are: Fe_2O_3–Fe_3O_4 (HM; Myers and Eugster, 1983), MnO–Mn_3O_4 (MHO; O'Neill and Pownceby, 1993b), Re–ReO_2 (RRO; Pownceby and O'Neill, 1994), Ni–NiO (NNO; O'Neill and Pownceby, 1993a) and iron–wüstite (IW; O'Neill, 1987).

gen buffer mixtures [hematite–magnetite (HM; Myers and Eugster, 1983), MnO–Mn_3O_4 (MHO; O'Neill and Pownceby, 1993b), Re–ReO_2 (RRO; Pownceby and O'Neill, 1994), Co–CoO (CCO; O'Neill and Pownceby, 1993a), Ni–NiO (NNO; O'Neill and Pownceby, 1993a) or quartz–fayalite–magnetite (QFM; O'Neill, 1987)]. The silica tubes were sealed and held in the hotspot of vertical resistance furnaces at atmospheric pressure, and then quenched by rapid removal from the furnace. Temperature was measured with a Type S ($Pt–Pt_{10}Rh$) thermocouple calibrated against the melting point of Au and with an uncertainty of ± 1 °C.

Four series of experiments were completed (Fig. 1 and Table 2). The first series was Cr_2O_3-doped and buffered at NNO. Significant amounts of NiO were introduced into the ankaramite due to NiO volatility from the buffers. These experiments were useful in evaluating the role of variable NiO on D(Ni) spinel/melt. A second series of experiments was carried out at

Table 2
Summary of experimental run conditions

Run#	T (°C)	Log fO_2, buffer	Comp.	Dopant	Time (h)	Experimental/predicted olivine Fo	Phases
Series 1							
178	1150	−8.16, NNO	1	1 wt.% Cr_2O_3	84	87/87	gl, sp, ol
179	1200	−7.56, NNO	1	1 wt.% Cr_2O_3	84	86/86	gl, sp, ol
172	1216	−7.38, NNO	1	1 wt.% Cr_2O_3	72	88/90	gl, sp, ol
174	1237	−7.15, NNO	1	1 wt.% Cr_2O_3	48	–	gl, sp
184	1260	−6.90, NNO	1	1 wt.% Cr_2O_3	24	87/87	gl, sp, ol
173	1298	−6.51, NNO	1	1 wt.% Cr_2O_3	48	–	gl, sp
177	1325	−6.24, NNO	1	1 wt.% Cr_2O_3	48	–	gl, sp
Series 2							
180	1300	−1.65, HM	1	1 wt.% Cr_2O_3	24	–	gl, sp
182	1300	−3.03, MHO	1	1 wt.% Cr_2O_3	24	–	gl, sp
198	1300	−5.07, RRO	1	1 wt.% Cr_2O_3	24	–	gl, sp
173	1298	−6.51, NNO	1	1 wt.% Cr_2O_3	48	–	gl, sp
199	1300	−7.18, QFM	1	1 wt.% Cr_2O_3	24	–	gl (q), sp
183	1300	−8.28, CCO	1	1 wt.% Cr_2O_3	46	89/88	gl, sp, ol
Series 3							
191	1150	−4.64, MHO	1	1 wt.% Cr_2O_3	113	88/91	gl, sp, ol, pl, cpx
196	1175	−4.35, MHO	1	1 wt.% Cr_2O_3	120	90/90	gl, sp, ol, cpx
190	1200	−4.07, MHO	1	1 wt.% Cr_2O_3	39	90/90	gl, sp, ol
193	1225	−3.80, MHO	1	1 wt.% Cr_2O_3	41	89/89	gl, sp, ol, cpx
189	1250	−3.53, MHO	1	1 wt.% Cr_2O_3	69	–	gl, sp
192	1275	−3.28, MHO	1	1 wt.% Cr_2O_3	42.5	–	gl, sp
182	1300	−3.03, MHO	1	1 wt.% Cr_2O_3	24	–	gl, sp
194	1325	−2.79, MHO	1	1 wt.% Cr_2O_3	24	–	gl, sp
Series 4							
189	1250	−3.53, MHO	1	1 wt.% Cr_2O_3	69	–	gl, sp
201	1250	−3.53, MHO	1	3 wt.% $MgAl_2O_4$	31	–	gl, sp
202	1250	−3.53, MHO	1	3 wt.% $FeFe_2O_4$	31	–	gl, sp
Leeman (1974) experiments							
T13	1252	−0.68	2	Undoped, NiO, CoO	69	96/97	gl, sp, ol
T3	1300	−0.68	2	Undoped, NiO, CoO	145	94–95/96	gl, sp, ol
T9	1151	−7.06	3	Undoped, NiO, CoO	61	72–75/77	gl, sp, ol
T6	1180	−0.91	3	Undoped, NiO, CoO	115	89–90/97	gl, sp, ol
T5	1248	−6.45	2	Undoped, NiO, CoO	75	86/87	gl, sp, ol
T11	1275	−5.98	2	Undoped, NiO, CoO	65	87–89/88	gl, sp, ol
T14	1250*	−6.00	3	Undoped, NiO, CoO	79	83–85/85	gl, sp, ol

Buffer abbreviations are as follows: HM: hematite–magnetite, MHO: MnO–Mn_3O_4, RRO: Re–ReO_2, CCO: Co–CoO, NNO: Ni–NiO and QFM: quartz–fayalite–magnetite.
Runs 173 and 189 are listed twice as parts of two series.
* Equilibrated at 1150 °C for 96 hours, before final hold at 1250 °C.

1300 °C on Cr_2O_3-doped ankaramite, with variable fO_2 controlled at the HM, MHO, RRO, NNO, QFM and CCO buffers. The third series of experiments was conducted between 1150 and 1325 °C at the MHO buffer, to assess the effect of temperature on the partitioning. A fourth series explored the effect of adding Cr_2O_3, $MgAl_2O_4$ and Fe_3O_4 to the ankaramite at 1250 °C, at the MHO buffer (Table 2).

In addition, experimental run products from the study of Leeman (1974) (cf. Leeman and Lindstrom, 1978) were analyzed. Although the focus of that study was olivine–melt partitioning of Ni and Co in picritic and tholeiitic compositions (Tables 1 and 2), many of the runs also contained spinels. Spinels were analyzed from seven series of experiments, between 1150 and 1300 °C (Fig. 1). Each series consists of five separate samples: one undoped composition, and four doped with 1% and 2% of NiO and 1% and 2% CoO. Oxygen fugacity was close to air for three of the series and approximately 1 log fO_2 unit above NNO for the four other series (see Table 2). Melt $Fe^{3+}/\sum Fe$ was determined from spinel chemistry (in the undoped charge) following Maurel and Maurel (1983), then used to calculate melt fO_2 (± 0.2 log fO_2 units; Table 2) using the calibration of Kress and Carmichael (1991).

Glasses and oxides were also synthesized for use as calibration standards for SIMS analysis. Glass of Di–An eutectic composition was synthesized from high purity CaO, MgO, Al_2O_3 and SiO_2 at 1 bar and 1400 °C; fusion and grinding of the glass was repeated several times to ensure homogeneity. Aliquots of this glass were doped with variable amounts of V, equilibrated at 1350 °C in sealed Pt capsules in a vertical furnace through which air was flowing. A series of three magnetite standards, containing variable amounts of CoO and V_2O_5, was synthesized in a piston cylinder apparatus (using the procedure described by Righter et al., 1997). Magnetite from the Minas-Gerais mine, Brazil, was used together with reagent grade CoO and V_2O_5; mixtures of magnetite and oxide were welded into Pt capsules, and equilibrated at 10 kbar and 1300 °C for 24 h. The magnetite standards and the V-bearing glasses we synthesized were analyzed by both electron and ion microprobes (Table 5). Together with Co- and Ni-bearing glasses from the studies of Leeman (1974) and Righter et al. (2004) (un-italicized values in Tables 3 and 4), these were used to build

Table 3
Electron and ion (italicized) probe analyses of glasses (average of *n* analyses)

Run	*n*	SiO_2	TiO_2	Al_2O_3	Cr_2O_3	FeO*	MnO	MgO	CaO	Na_2O	K_2O	P_2O_5	CoO	NiO	V (ppm)	Total
178	15	46.72	3.40	15.20	0.04	8.87	0.39	6.67	11.41	3.51	1.15	0.53	*0.012(1)*	0.26(8)	*540(54)*	98.16
179	15	46.58	3.48	14.31	0.05	9.42	0.20	8.10	12.30	1.70	0.76	0.44	*0.014(1)*	0.54(3)	*520(52)*	97.89
172	10	46.16	3.85	14.85	0.10	7.60	–	9.61	12.78	1.65	0.46	0.42	*0.0033(3)*	*0.023(2)*	*310(31)*	97.48
174	20	46.83	3.36	13.89	0.16	8.83	–	9.88	12.15	2.11	0.85	0.39	*0.0086(9)*	*0.049(5)*	*430(43)*	98.44
184	15	49.04	3.41	13.52	0.17	6.44	0.20	12.47	12.62	1.02	0.23	0.41	*0.12(1)*	*0.62(6)*	*1050(110)*	99.65
173	19	46.28	3.23	12.81	0.13	9.63	–	11.44	12.30	1.01	0.33	0.33	*0.0033(3)*	*0.091(9)*	*330(33)*	97.50
177	13	51.74	2.57	21.90	0.13	5.33	0.11	6.88	7.98	1.25	0.24	0.30	*0.0058(6)*	0.38(7)	*330(33)*	98.83
180	14	43.97	3.00	12.57	0.13	12.13	0.20	10.44	11.18	2.36	0.61	0.37	*0.034(3)*	*0.14(1)*	*410(41)*	97.03
182	5	44.17	3.01	12.16	0.06	11.63	0.27	10.97	11.65	2.71	0.96	0.37	*0.019(2)*	*0.029(3)*	*280(28)*	98.02
198	10	46.69	3.22	12.85	0.11	11.90	0.22	10.62	11.21	0.03	0.01	0.36	*0.015(2)*	*0.058(6)*	*480(48)*	97.26
173	19	46.28	3.23	12.81	0.13	9.63	–	11.44	12.30	1.01	0.33	0.33	*0.0033(3)*	*0.091(9)*	*330(33)*	97.50
199	10	44.92	3.07	12.52	0.10	11.02	0.22	10.37	11.64	2.65	0.91	0.41	*0.024(2)*	*0.033(3)*	*470(47)*	97.86
183	15	59.81	2.44	12.30	0.31	1.35	0.03	13.52	9.25	0.92	0.20	0.25	0.34(3)	*0.63(6)*	*46(5)*	100.71
191	15	49.74	4.07	12.98	0.04	9.10	0.36	8.09	11.23	2.28	0.62	0.75	*0.016(2)*	*0.018(2)*	*75(8)*	99.28
196	10	47.97	3.31	14.02	0.03	8.70	0.19	7.65	11.88	2.87	1.07	0.48	*0.0027(3)*	*0.93(9)*	*170(17)*	98.21
190	15	48.03	3.19	12.62	0.04	8.49	0.46	9.63	12.84	2.20	0.78	0.37	*0.016(2)*	*0.0034(3)*	*580(58)*	98.66
193	13	47.39	3.06	12.10	0.04	8.99	0.19	10.31	12.14	1.69	0.68	0.44	*0.013(1)*	*0.0076(8)*	*570(57)*	97.07
189	20	46.59	2.97	11.36	0.05	9.98	0.18	11.93	11.85	2.02	0.64	0.32	*0.019(2)*	*0.037(4)*	*530(53)*	97.91
192	15	46.58	3.15	12.45	0.08	9.76	0.18	10.66	13.20	1.92	0.54	0.37	*0.023(2)*	*0.043(4)*	*540(54)*	98.91
182	5	44.17	3.01	12.16	0.06	11.63	0.27	10.97	11.65	2.71	0.96	0.37	*0.019(2)*	*0.029(3)*	*280(28)*	98.02
194	12	44.82	3.11	12.56	0.11	11.15	0.19	10.34	11.51	2.32	0.66	0.41	*0.014(1)*	*0.021(2)*	*550(55)*	97.20
189	20	46.59	2.97	11.36	0.05	9.98	0.18	11.93	11.85	2.02	0.64	0.32	*0.019(2)*	*0.037(4)*	*530(53)*	97.91
201	10	42.98	2.95	13.85	0.01	11.92	0.22	10.82	11.44	2.30	0.61	0.37	*0.017(2)*	*0.041(4)*	*500(50)*	97.49
202	10	43.95	2.88	11.94	0.01	13.73	0.19	10.85	11.33	1.88	0.42	0.40	*0.025(3)*	*0.064(6)*	*430(43)*	97.64

Numbers in parentheses represent the standard deviation from the mean of the analyses for each run; standard deviations for major elements are typically 2% or less.

Underlined concentrations are unusually low and correspond to anomalously high *D* values.

Table 4
Electron and ion (italicized) probe analyses of glasses (average of *n* analyses)

Run	*n*	SiO_2	TiO_2	Al_2O_3	Cr_2O_3	FeO[a]	MnO	MgO	CaO	Na_2O	K_2O	P_2O_5	CoO	NiO	V (ppm)	Total
T13-1	–	48.55	2.36	10.92	–	11.74	–	11.03	10.22	1.66	0.43	–	*0.0094(9)*	*0.039(4)*	*160(16)*	96.95
T13-2	–	50.25	2.33	11.8	–	9.88	–	9.93	11.09	2.01	0.46	–		0.55(5)	–	98.30
T13-3	–	49.07	2.3	10.87	–	10.42	–	10.08	10.84	1.82	0.41	–	1.47(7)	–	–	97.28
T13-4	–	48.53	2.33	10.69	–	11.12	–	10.5	10.72	1.89	0.46	–	0.88(5)	*0.053(5)*	*160(16)*	97.17
T13-5	–	48.63	2.41	12.84	–	10.64	–	10.39	10.85	1.55	0.43	–	1.49(8)	*0.043(4)*	*160(16)*	99.27
T3-2	–	46.17	1.03	10.7	–	12.75	–	12.25	9.97	1.5	0.34	–	*0.0094(9)*	0.52(5)	*140(14)*	95.23
T3-3	–	47.34	1.13	10.93	–	11.62	–	11.68	12.27	1.53	0.35	–	*0.010(1)*	0.98(9)	*140(14)*	97.83
T9-1	–	47.62	3.72	12.75	–	14.33	–	5.82	9.27	2.66	0.93	–	*0.0068(7)*	*0.027(3)*	*200(20)*	97.13
T9-2	–	47.99	3.93	12.27	–	14.23	–	4.89	9.76	2.69	0.99	–		0.41(4)	–	97.16
T9-3	–	49.3	3.83	13.3	–	12.77	–	4.15	10.49	2.76	1.12	–	*0.032(3)*	0.85(8)	*190(19)*	98.57
T9-4	–	47.2	3.67	12.94	–	13.89	–	5.22	8.58	2.6	0.89	–	0.99(5)	*0.036(4)*	*200(20)*	96.02
T9-5	–	47.45	3.64	13.01	–	13.81	–	5.19	9.49	2.62	0.95	–	1.88(9)	*0.046(5)*	*180(18)*	98.04
T6-1	10	52.63	2.20	14.31	0.021	7.45	0.22	8.15	10.02	2.66	0.78	0.60	*0.014(1)*	*0.020(2)*	*220(20)*	99.05
T6-2	10	53.72	3.03	13.80	0.017	6.46	0.16	7.16	10.44	2.63	0.80	0.56	0.014(1)	0.31(4)	–	99.10
T6-3	10	54.19	3.11	13.86	0.012	5.57	0.20	6.40	10.90	2.59	0.81	0.63	*0.014(1)*	0.64(8)	*240(24)*	98.91
T6-4	10	53.15	2.86	14.22	0.014	7.07	0.18	7.32	10.13	2.66	0.76	0.55	0.74(4)	*0.021(2)*	*210(21)*	99.67
T6-5	9	52.65	3.03	14.02	0.019	6.80	0.18	7.05	10.24	2.60	0.79	0.43	1.06(10)	*0.023(2)*	*230(23)*	98.87
T5-1	–	48.72	1.85	12.41	–	11.01	–	9.01	11.08	1.84	0.48	–	*0.0066(7)*	*0.041(4)*	*180(18)*	96.44
T5-2	–	48.73	2.02	12.46	–	10.93	–	8.49	11.38	1.92	0.5	–	–	0.16(2)	–	96.59
T5-3	–	48.69	2.16	12.59	–	10.94	–	8.3	11.59	1.98	0.51	–	–	0.45(4)	–	97.21
T5-4	–	48.43	2.23	12.41	–	10.91	–	8.6	11.22	1.87	0.48	–	0.71(3)	–	*170(17)*	96.86
T5-5	–	48.07	2.41	12.35	–	10.82	–	8.62	11.02	1.81	0.48	–	1.61(8)	*0.044(4)*	*180(18)*	97.23
T11-1	–	48.66	2.5	11.43	–	11.77	–	10.76	10.96	1.8	0.42	–	*0.0076(8)*	*0.091(9)*	*180(18)*	98.39
T11-2	–	46.52	2.56	11.55	–	11.14	–	10.29	11.11	1.94	0.45	–		–	–	95.83
T11-3	–	48.21	2.59	11.79	–	11.61	–	9.84	11.12	1.88	0.43	–	*0.027(3)*	–	*180(18)*	98.15
T11-4	–	48.03	2.47	11.34	–	11.05	–	10.33	12.9	1.86	0.46	–	1.47(2)	*0.044(4)*	*180(18)*	99.95
T11-5	–	47.96	2.45	11.38	–	11.51	–	10.23	10.64	1.79	0.42	–	1.57(7)	*0.051(5)*	*170(17)*	98.00
T14-1	9	49.77	2.77	14.79	0.009	10.22	0.22	7.42	9.96	2.47	0.70	0.44	*0.013(1)*	*0.024(2)*	*160(16)*	98.82
T14-2	10	51.05	3.00	14.26	0.014	8.53	0.14	7.27	10.11	2.45	0.69	0.43	*0.060(6)*	0.46(5)	*170(17)*	98.45
T14-3	10	52.55	2.76	14.21	0.017	6.44	0.19	7.28	10.52	2.56	0.71	0.51	*0.029(3)*	1.28(9)	*190(19)*	99.07
T14-4	10	50.54	2.83	14.43	0.015	9.13	0.19	6.91	9.88	2.56	0.71	0.35	1.55(8)	*0.038(4)*	*180(18)*	99.16
T14-5	10	50.28	2.79	14.38	0.006	7.98	0.15	7.02	9.87	2.45	0.67	0.41	2.67(11)	*0.045(5)*	*170(17)*	98.71

Numbers in parentheses represent the standard deviation from the mean of the analyses for NiO, CoO and V.

[a] T6 and T14 major element analyses are new; all other major element glass analyses are from Leeman (1974); data reported from these runs typically represent an average of five spot analyses; standard deviations for major elements are typically 2% or less.

Table 5
Microprobe analyses of oxides and glasses used for V and Co SIMS calibrations

	A	B	C	D	E	1	2	3
	Glasses[a]					Oxides		
SiO_2	46.77	47.03	46.64	46.11	46.08	0.10	0.12	0.13
TiO_2	–	–	–	–	–	0.09	0.15	0.10
Al_2O_3	15.36	15.45	15.25	15.14	15.14	0.18	0.18	0.15
Cr_2O_3	–	–	–	–	–	0.01	0.14	0.06
FeO*	–	–	–	–	–	92.34	88.75	90.00
MgO	9.59	9.64	9.64	9.50	9.43	0.21	0.08	0.10
Na_2O	0.99	0.93	1.00	0.99	0.98	–	–	–
CaO	21.98	21.92	21.88	21.68	21.66	–	–	–
CoO	–	–	–	–	–	0.015	1.66	1.14
V_2O_3	0.00	0.24	0.54	0.95	1.24	0.15	2.29	1.04
Total	94.69	95.21	94.95	94.37	94.53	93.19	93.46	92.81

[a] Low totals reflect a small amount of WO_2 that was observed in energy spectra.

SIMS calibration curves for V, Co and Ni in glass and V and Co in spinel.

3. Analytical techniques

All major elements, Ni in spinels, and Ni and Co in some glasses, were analyzed with a CAMECA SX50 electron microprobe, using an accelerating voltage of 15 kV and sample current of 10 nA. Standards include both natural (albite, diopside, potassium feldspar, fayalite, rhodonite, apatite, chromite) and synthetic (Ni, Co, V, TiO_2) materials. Counting times for major elements was typically 10 s and as long as 120 s for minor elements (Ni and Co). Under these conditions, detection limits were approximately 100 ppm for Ni, Co and V. PAP ϕ–ρ–Z corrections were used in the data reduction (Pouchou and Pichoir, 1991). FeO and Fe_2O_3 in spinels were calculated by charge balance and stoichiometry

Table 6
Electron microprobe and ion (italicized) probe analyses of spinels (average of n analyses)

Run	n	SiO_2	TiO_2	Al_2O_3	Cr_2O_3	FeO_t	MnO	MgO	CoO	NiO	V (ppm)	FeO[a]	Fe_2O_3[a]	Total
178	7	0.27	5.62	13.86	11.35	47.33	0.39	10.50	*0.028(3)*	5.89(11)	*370(37)*	16.56	34.19	98.77
179	3	0.13	4.64	20.31	23.26	29.78	0.00	10.90	*0.018(2)*	8.50(4)	*640(64)*	14.18	17.34	99.39
172	6	–	2.56	25.41	34.64	18.07	0.43	16.02	–	0.68(6)	–	12.18	6.54	98.47
174	20	–	1.50	26.59	30.89	23.20	0.37	15.21	*0.015(2)*	0.15(4)	*620(62)*	13.33	10.97	99.01
184	15	0.17	1.10	27.31	32.84	22.51	–	15.77	*0.015(2)*	0.20(6)	*420(42)*	13.38	10.14	100.93
173	5	–	3.43	24.10	29.74	21.08	0.36	14.63	*0.021(2)*	3.89(12)	*320(32)*	11.71	10.42	98.28
177	12	0.16	2.22	32.82	30.31	12.97	0	15.68	*0.020(2)*	4.34(14)	*440(44)*	10.85	2.36	98.94
180	4	0.10	1.90	13.62	27.95	37.68	0.23	14.14	*0.042(4)*	0.57(3)	*290(29)*	12.86	27.58	99.01
182	12	0.15	1.72	11.24	17.66	48.55	0.026	14.80	–	0.21(6)	–	11.57	41.10	98.47
198	4	0.10	0.99	10.23	19.70	44.78	0.18	17.97	*0.027(3)*	0.34(8)	*20(2)*	5.57	43.57	98.66
173	5	–	3.43	24.10	29.74	21.08	0.36	14.63	*0.021(2)*	3.89(12)	*320(32)*	11.71	10.42	98.28
199	4	0.31	2.24	16.91	34.39	27.64	0.00	14.79	*0.022(2)*	0.09(4)	*260(26)*	13.54	15.67	97.99
183	6	0.07	0.84	23.86	48.77	1.75	0.41	20.83	2.05(8)	–	*70(7)*	1.33	0.70	99.93
191	5	0.09	4.14	9.49	16.12	51.69	0.70	12.83	*0.039(4)*	0.14(3)	*190(19)*	16.05	39.61	99.20
196	10	0.10	2.73	10.28	12.14	54.92	0.34	13.44	*0.050(5)*	0.22(4)	*380(38)*	14.05	45.42	98.77
190	10	0.14	1.62	9.16	8.55	53.76	0.41	19.01	*0.041(4)*	0.27(2)	*110(11)*	4.02	55.27	98.46
193	3	0.09	1.30	9.68	14.95	48.47	0.21	18.84	*0.039(4)*	0.28(4)	*80(8)*	4.39	48.99	98.74
189	20	0.12	1.31	11.55	15.94	45.55	0.40	19.12	*0.020(2)*	0.28(3)	*190(19)*	4.22	45.93	98.87
192	2	0.38	1.09	10.53	19.51	44.92	0.13	18.76	*0.034(3)*	0.22(4)	*210(21)*	5.13	44.22	99.78
182	12	0.15	1.72	11.24	17.66	48.55	0.026	14.80	–	0.21(6)	–	11.57	41.10	98.47
194	4	0.10	1.14	11.10	17.55	46.24	0.16	17.94	*0.033(3)*	0.27(5)	*220(22)*	6.07	44.64	98.99
189	20	0.12	1.31	11.55	15.94	45.55	0.40	19.12	*0.020(2)*	0.28(3)	*190(19)*	4.22	45.93	98.87
201	8	0.17	2.33	16.04	2.10	57.63	0.24	15.00	*0.033(3)*	0.33(3)	*55(6)*	12.28	50.39	98.91
202	7	0.12	2.06	8.83	5.42	63.19	0.23	12.33	*0.030(3)*	0.32(6)	*50(5)*	14.57	54.03	97.94

Numbers in parentheses represent the standard deviation from the mean of the analyses for NiO, CoO and V; standard deviations for all other elements are typically 2% or less.

[a] FeO and Fe_2O_3 recalculated from total iron as FeO (FeO_t) according to charge balance and stoichiometry.

(Carmichael, 1967) and spinel compositions were calculated to three cations for use in plotting (e.g., X_{Ti} refers to the amount of Ti calculated around three cations). All analyses are reported in Tables 3–7.

Glasses containing concentrations of Ni, Co and V close to, or below, detection limits of electron microprobe analysis (~100 ppm) were analyzed subsequently using secondary ion mass spectrometry (SIMS) with CAMECA 3f and 6f ion probes at Arizona State University. Previous SIMS work on Ni by Steele and Lindstrom (1981) was used as a guide for our analyses. SIMS analyses of silicate glass were obtained using a ~1 nA primary beam of $^{16}O^-$ focused to a spot 10–15 μm in diameter. Positive secondary ions with initial kinetic energies of 0–40 eV were accelerated into the mass spectrometer. To minimize molecular interferences on V, Co and Ni, the mass spectrometer was operated at high mass resolving power (~5000). For example, $^{51}V^+$ was resolved from $^{24}Mg^{27}Al^+$, $^{59}Co^+$ from $^{29}Si^{30}Si^+$ and $^{60}Ni^+$ from $^{30}Si_2^+$. The minor isotope of nickel was used because it is not possible to resolve the ^{58}Fe ion from ^{58}Ni (the most abundant Ni isotope). Each analysis consisted of a 5 min pre-sputter period followed by collection of secondary ion intensities for ^{30}Si, ^{51}V, ^{59}Co and ^{60}Ni for time sufficient to reach integrated signals of at least 100 (and typically 500) counts. Calibration curves for Ni, Co and V in glass and Co and V in spinel in magnetite are shown in Figs. 2 and 3. The V-doped Di–An eutectic composition glasses were also used to check for interference of $^{24}Mg^{27}Al$ with ^{51}V. Nickel, Co and V contents measured by ion probe are presented in (Tables 3, 4, 6 and 7). Typical error on a SIMS trace element analysis is 10%, which corresponds to 20% for a partition coefficient, and is attributable mainly to counting statistics. Reproducibility of the measurements is demonstrated by repeat analysis of

Table 7
Electron microprobe analyses of spinels from runs of Leeman (1974) (average of *n* analyses)

Run	*n*	TiO_2	Al_2O_3	Cr_2O_3	FeO_t	MnO	MgO	CoO	NiO	V_2O_3	FeO[a]	Fe_2O_3[a]	Total
T13-1	10	1.33	6.55	1.82	66.61	0.27	15.59	0.03(01)	0.82(03)	0.04(02)	8.20	64.91	99.56
T13-2	8	1.41	6.46	0.85	63.48	0.23	13.03	–	6.94(11)	0.05(03)	6.07	63.80	98.85
T13-3	9	1.69	6.48	1.19	62.74	0.23	12.55	7.74(16)	0.58(06)	0.06(02)	5.88	63.18	99.59
T13-4	8	1.49	6.48	1.23	64.82	0.24	13.61	4.90(07)	0.92(04)	0.06(02)	6.72	64.57	100.22
T13-5	7	1.66	6.61	1.15	62.24	0.24	12.64	7.62(11)	0.57(06)	0.05(02)	5.70	62.83	99.07
T3-2	8	1.33	7.43	2.51	60.73	0.21	12.57	–	8.20(10)	0.07(04)	5.80	61.04	99.16
T3-3	8	1.57	7.68	2.08	58.00	0.19	10.35	–	13.22(25)	0.04(01)	4.59	59.36	99.07
T9-1	10	10.86	6.46	4.09	66.15	0.31	6.10	–	0.26(03)	0.82(05)	32.03	37.92	98.85
T9-2	10	12.86	5.25	0.24	62.72	0.27	4.44	–	8.11(07)	0.79(06)	28.45	38.09	98.51
T9-3	6	14.97	5.47	0.31	54.03	0.27	3.88	0.09(05)	15.09(20)	0.95(04)	24.40	32.92	98.36
T9-4	10	10.85	9.24	2.43	60.54	0.25	5.83	4.92(11)	0.21(03)	0.77(03)	28.10	36.05	98.65
T9-5	10	13.24	5.68	0.92	59.78	0.26	4.89	8.99(12)	0.17(05)	0.88(03)	27.08	36.34	98.45
T6-1	10	1.56	9.08	0.69	63.39	0.53	17.02	0.04(02)	0.39(03)	0.07(03)	6.64	63.06	99.08
T6-2	10	2.40	8.22	0.11	58.70	0.39	12.10	–	11.25(26)	0.09(02)	4.51	60.22	99.29
T6-3	10	2.92	7.97	0.12	53.63	0.34	8.92	0.08(03)	18.17(34)	0.10(03)	2.66	56.64	97.92
T6-4	10	2.22	8.15	0.79	60.81	0.43	13.92	7.04(13)	0.15(04)	0.10(04)	5.51	61.45	99.76
T6-5	10	2.53	7.85	0.92	58.65	0.40	12.66	9.47(16)	0.31(07)	0.11(02)	4.90	59.73	98.88
T5-1	10	2.30	15.00	34.32	30.47	0.38	12.45	–	0.30(07)	0.29(03)	15.63	16.49	97.15
T5-2	10	2.90	12.81	37.63	29.60	0.41	11.80	–	1.63(18)	0.27(05)	15.96	15.16	98.57
T5-3	10	2.78	12.14	37.56	28.59	0.39	9.51	–	4.60(38)	0.25(05)	16.13	13.85	97.71
T5-4	10	1.82	10.96	42.91	27.43	0.42	10.45	2.94(06)	0.78(10)	0.22(03)	14.95	13.87	99.32
T5-5	10	3.07	15.12	33.79	27.71	0.34	10.63	6.42(12)	0.22(08)	0.30(03)	13.57	15.72	99.17
T11-1	9	1.88	12.79	39.28	30.13	0.36	12.68	–	0.57(06)	0.17(02)	15.05	16.75	99.55
T11-2	10	2.44	14.30	36.48	28.61	0.36	12.67	–	2.56(07)	0.22(02)	13.80	16.46	99.30
T11-3	8	2.87	14.48	31.06	29.85	0.32	10.95	0.07(03)	5.69(19)	0.23(03)	13.13	18.58	97.38
T11-4	8	2.33	14.66	35.77	27.41	0.34	11.71	5.26(15)	0.19(04)	0.21(01)	12.46	16.62	99.54
T11-5	10	2.40	14.43	33.90	28.47	0.31	11.52	5.50(10)	0.25(05)	0.20(02)	12.24	18.03	98.79
T14-1	9	11.55	2.67	0.34	73.27	0.10	3.82	–	0.07(04)	0.40(08)	35.11	42.41	96.47
T14-2	9	2.06	8.85	0.27	59.48	0.29	10.22	0.35(03)	11.80(29)	0.08(03)	6.43	58.96	99.30
T14-3	10	3.04	10.27	0.09	51.51	0.23	7.11	0.10(03)	21.82(21)	0.12(03)	3.05	53.86	99.68
T14-4	9	2.12	8.66	0.27	61.12	0.31	10.14	10.47(15)	0.39(05)	0.06(02)	7.74	59.32	99.48
T14-5	9	2.42	8.71	0.41	56.66	0.27	9.05	15.68(21)	0.18(04)	0.09(01)	4.75	57.68	99.25

[a] FeO and Fe_2O_3 recalculated from total iron as FeO (FeO_t) according to charge balance and stoichiometry; numbers in parentheses represent the standard deviation from the mean of the analyses for NiO, CoO and V; standard deviations for all other elements are typically 2% or less. (−1) undoped, (−2) 1 wt.% Ni, (−3) 2 wt.% Ni, (−4) 1 wt.% Co, (−5) 2 wt.% Co; except for T13 where −2 is Ni and −3, −4 and −5 have Co.

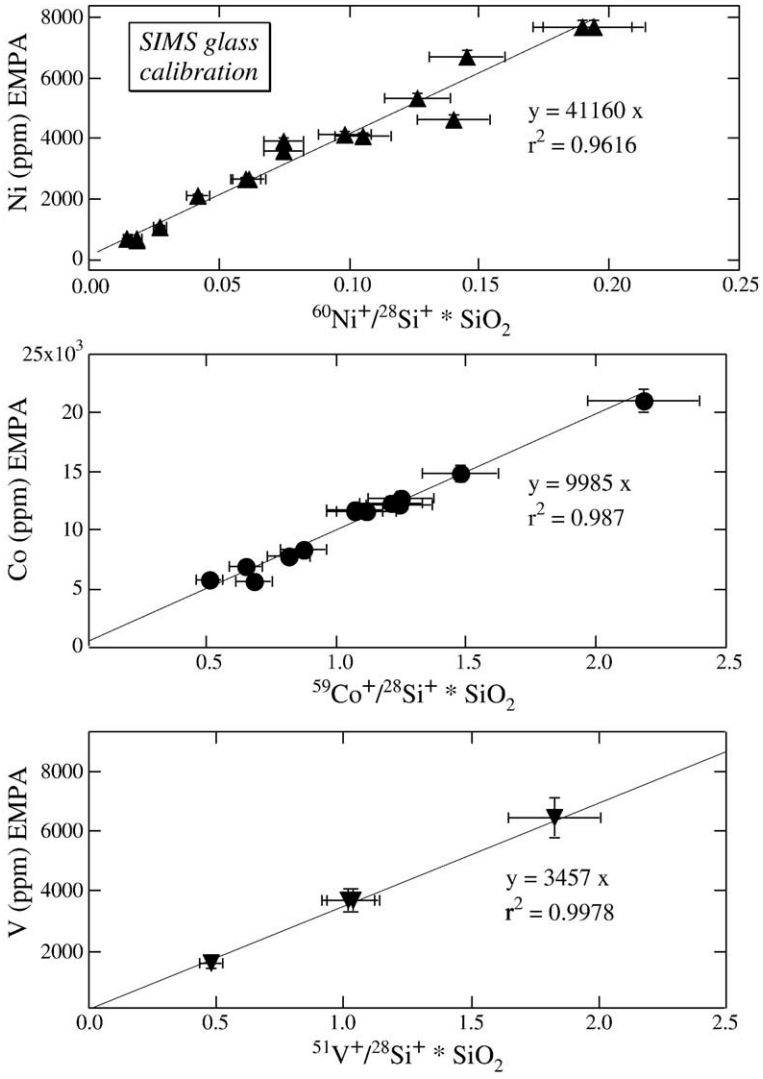

Fig. 2. SIMS calibration for Ni, Co and V in glasses. For Ni, glasses T3-2, T3-3, T6-3, T9-3, T11-3 and T14-2 from Leeman (1974), and 158A, 159A, 160A, 162A, 162B, 164A, 165A and 167A from Righter et al. (2004) were used for the calibration. For Co, glasses T5-4, T5-5, T6-4, T6-5, T-4, T9-5, T11-4, T11-5, T13-4, T13-5, T14-2, -3, -4 and -5 from Leeman (1974) were used for calibration (Table 3). For V, glasses in Table 5 were used for calibration. Analysis conditions are discussed in the text.

two glasses (Table 8). Spinels in the undoped experiments have Co and V concentrations below detection limits for the electron microprobe (~100 ppm), and were analyzed using SIMS. SIMS analyses were obtained as with silicates (using high mass resolution conditions to resolve $^{51}V^{+}$ from $^{24}Mg^{27}Al^{+}$), but with $^{56}Fe^{+}$ replacing $^{30}Si^{+}$ as a normalizing isotope.

Two aspects of the SIMS analyses justify elaboration: agreement between EMPA and SIMS analyses, and whether the calibration curves remain linear at low concentrations. First, several glasses were analyzed for Ni and Co by EMPA and SIMS, but not included in the calibration. Comparison of their concentrations (Table 9) shows that the agreement is within the uncertainty of each measurement, demonstrating excellent agreement between these techniques. Second, the calibration curves for Ni, Co and V are constructed at concentration levels higher than those of the unknowns. Several previous studies have shown that concentration–intensity curves remain linear down to very low concentrations (Steele et al., 1981; Shimizu et al., 1978).

4. Results and discussion

All runs contain spinel and glass, and some (at lower temperatures) also contain olivine, clinopyroxene and

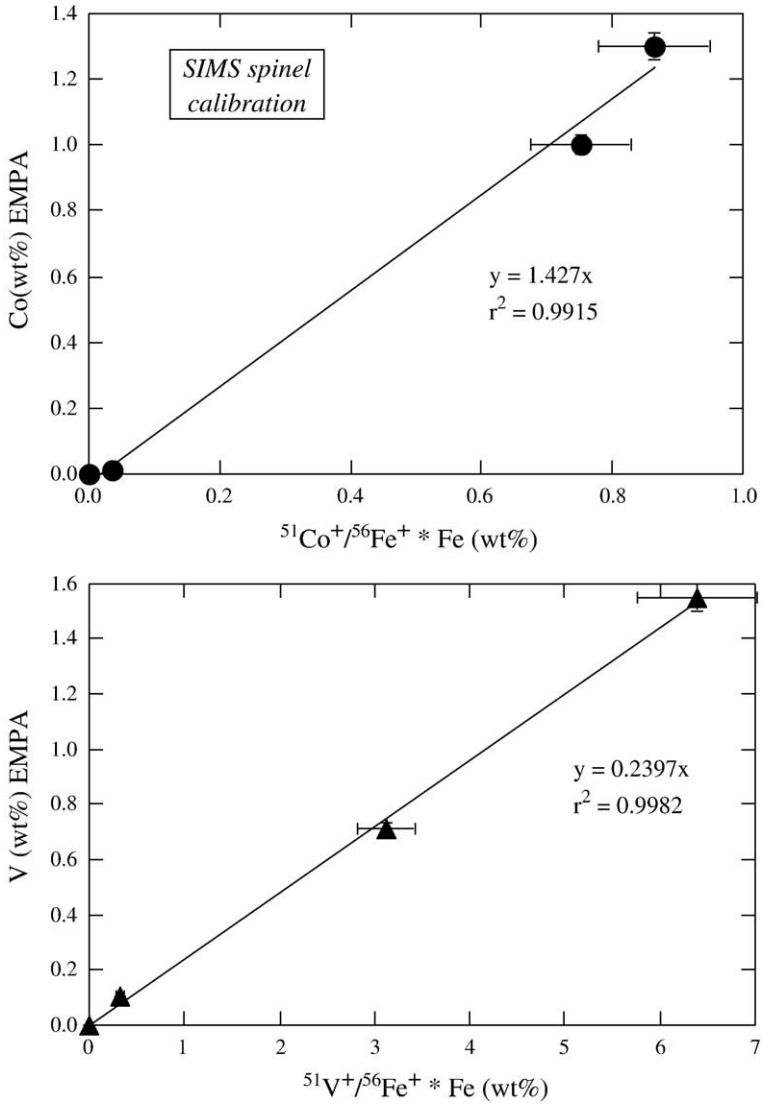

Fig. 3. SIMS calibration for Co and V in spinels. Spinel compositions presented in Table 5 were used for calibration of V and Co. Analysis conditions are discussed in the text.

plagioclase (see Fig. 4). Some spinels produced in our experiments contain a large amount of Cr, but there is a range of compositions produced by the variable oxygen fugacity (Tables 2 and 3; Fig. 5), from low (air) to high (NNO) $Cr/(Fe^{3+}+Cr+Al+Ti+V)$, from high (air) to low (NNO) $Fe^{3+}/(Fe^{3+}+Cr+Al+Ti+V)$ and variable $Ti/(Fe^{3+}+Cr+Al+Ti+V)$. A summary of all partition coefficients is presented in Table 10.

Table 8
Replicate analysis of glasses by SIMS

Run	$^{51}V^{+}/^{30}Si^{+}$	$^{59}Co^{+}/^{30}Si^{+}$	$^{60}Ni^{+}/^{30}Si^{+}$
T14-1-1	0.0283	0.00623	0.00277
T14-1-2	0.0281	0.00603	0.00270
T11-4-1	0.0322	0.691	0.00524
T11-4-2	0.0313	0.663	0.00499

Ratios were calculated from average of 20 s.
Counting cycles over a total of 10 to 15 min.

Table 9
Comparison of EMPA and SIMS analyses

Run	SIMS	EMPA
Nickel		
T14-2	3050 (200)	3590 (360)
162A	750 (80)	630 (65)
167	4030 (320)	4130 (410)
Cobalt		
T9-4	8180 (650)	7790 (780)
T13-1	12,100 (750)	12,300 (1200)
T14-4	12,450 (800)	12,200 (1200)

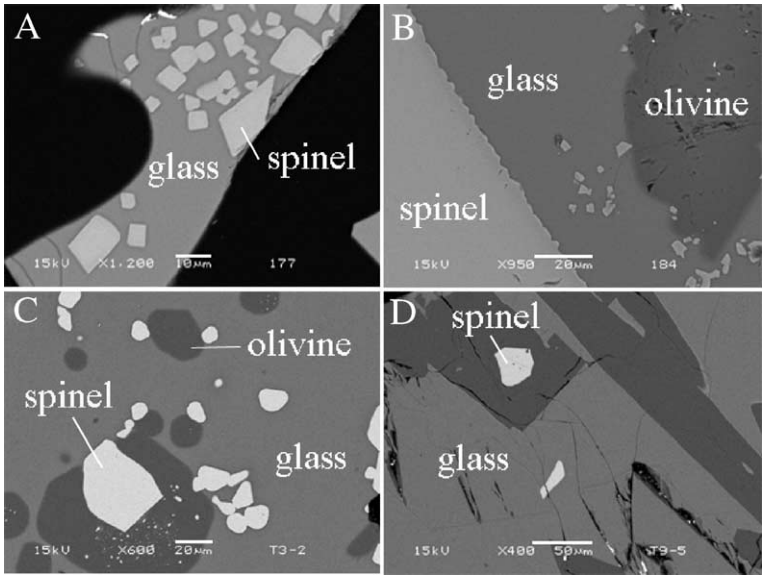

Fig. 4. Back scattered electron (BSE) images from four experiments from this study: (A) 177 run at 1325 °C, the NNO buffer and containing spinel and glass; (B) 184 run at 1260 °C, the NNO buffer, and containing olivine, spinel and glass; (C) T3-2 run at 1300 °C, in air, and containing olivine, spinel and glass; (D) T9-5 run at 1151 °C, near the QFM buffer and containing olivine, spinel and glass.

Before discussing the partitioning results, several notable aspects of spinel crystal chemistry must be reviewed (e.g., Waychunas, 1991; Papike et al., 2005). The spinel structure is very nearly a close-packed array of oxygen atoms where one third of the cations occupy tetrahedral sites (A sites) and two thirds occupy octahedral sites (B sites). Spinels are called "normal" if a doubly charged cation such as Fe^{2+} occupies only the

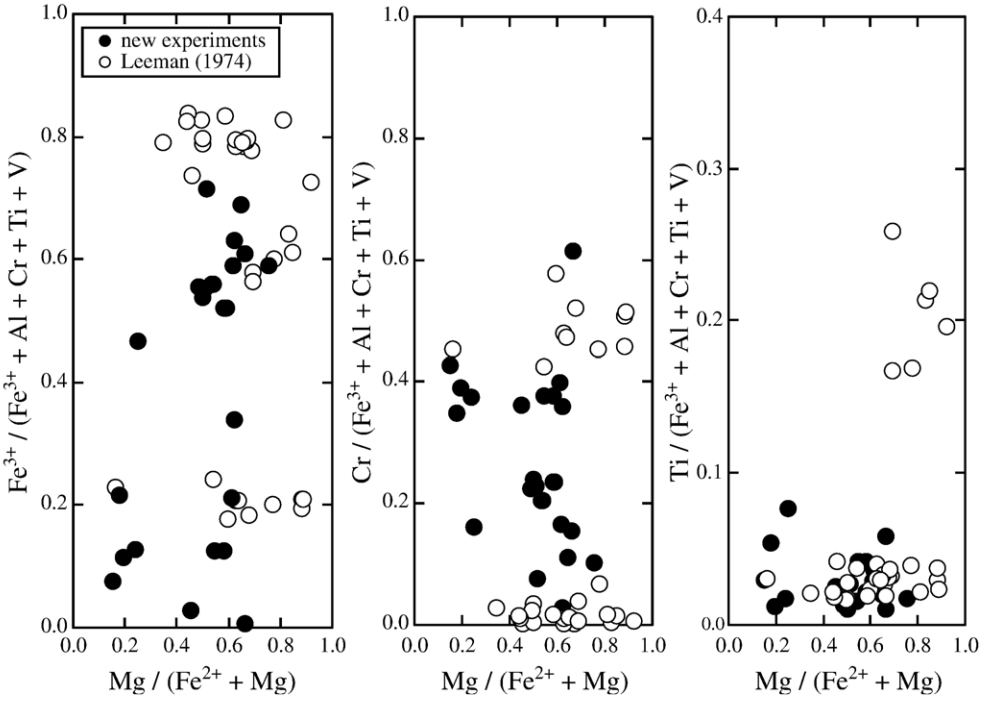

Fig. 5. Summary of spinel compositions from this study (solid circles) and Leeman (1974) experiments (open circles), in terms of $Fe^{3+}/(Fe^{3+}+Cr+Al+Ti+V)$, $Cr/(Fe^{3+}+Cr+Al+Ti+V)$ and $Ti/(Fe^{3+}+Cr+Al+Ti+V)$ vs. Mg# ($Mg/(Mg+Fe^{2+})$). Mg# is calculated using Fe^{2+} determined from spinel stoichiometry.

Table 10
Summary of partition coefficients

Run	D(Ni)	D(Co)	D(V)	Run	D(Ni)	D(Co)	D(V)
Series 1: all NNO, variable T							
178	22.6 (33, 17)	2.3 (2.8, 1.8)	0.68 (0.82, 0.56)	T13-1	21.0 (23.7, 18.3)	3.2 (4.6, 1.8)	1.7 (2.9, 0.5)
179	4.33 (12, 10.8)	1.3 (1.6, 1.0)	1.2 (1.5, 1.0)	T13-2	12.6 (15.2, 10.0)	–	–
172	29.6 (35, 25)	–	–	T13-3	–	5.3 (6.7, 3.9)	–
174	3.1 (4.3, 2.1)	1.7 (2.1, 1.3)	1.5 (1.8, 1.2)	T13-4	17.4 (19.8, 15.0)	5.6 (6.6, 4.6)	2.6 (3.8, 1.6)
184	–	–	0.40 (0.5, 0.33)	T13-5	13.3 (16.1, 10.5)	5.1 (6.2, 4.0)	2.2 (3.3, 1.1)
173	42.7 (49, 38)	6.4 (7.7, 5.1)	0.97 (1.2, 0.8)				
177	11.4 (14.5, 9.3)	3.4 (4.1, 2.7)	1.4 (1.7, 1.0)	T3-2	15.8 (19.0, 12.6)	–	3.5 (5.8, 1.2)
Series2: 1300 °C, variable fO_2				T3-3	13.5 (18.2, 8.8)	–	1.9 (2.4, 1.4)
180	4.1 (4.7, 3.1)	1.2 (1.5, 0.9)	0.72 (0.9, 0.6)				
182	7.2 (10.4, 4.7)	–	–	T9-1	9.6 (10.8, 8.4)	–	27.3 (31.7,22.9)
198	5.8 (6.9, 3.2)	1.8 (2.2, 1.4)	0.04 (0.05, 0.03)	T9-2	19.8 (23.2, 16.4)	–	–
173	42.7 (49, 38)	6.4 (7.7, 5.1)	0.97 (1.2, 0.8)	T9-3	17.8 (23.1, 12.5)	2.8 (3.2, 2.4)	33.9 (40.0, 27.8)
199	2.7 (3.5, 0.72)	0.93 (1.1, 0.7)	0.55 (0.68, 0.43)	T9-4	5.8 (6.6, 5.0)	5.0 (6.1, 3.9)	26.6 (30.3, 22.9)
183	–	6.0 (7.3, 4.7)	1.5 (1.9, 1.3)	T9-5	3.7 (4.3, 3.1)	4.8 (5.9, 3.7)	33.8 (38.5, 29.1)
Series 3: MHO buffer, variable T							
191	8.0 (11.3, 6.0)	2.4 (2.9, 1.9)	2.5 (3.2, 2.1)	T6-1	19.5 (23.0, 16.0)	2.9 (4.6, 1.2)	2.2 (2.7, 1.7)
196	–	18.5 (25, 15)[a]	2.3 (2.7, 1.8)	T6-2	36.3 (41.7, 30.9)	–	–
190	79.4 (93, 67)[a]	2.6 (3.2, 2.0)	0.18 (0.20, 0.16)	T6-3	28.4 (32.7, 24.1)	5.7 (8.4, 3.0)	2.8 (3.4, 2.2)
193	36.7 (44, 27)	3.0 (3.6, 2.4)	0.14 (0.17, 0.10)	T6-4	7.1 (9.7, 4.5)	9.5 (10.2, 8.8)	3.2 (3.9, 2.5)
189	7.6 (9.4, 6.3)	1.1 (1.3, 0.9)	0.35 (0.36, 0.30)	T6-5	13.5 (18.0, 9.0)	8.9 (9.9, 7.9)	3.3 (4.0, 2.6)
192	5.2 (7.2, 4.3)	1.5 (1.8, 1.2)	0.38 (0.47, 0.30)				
182	7.2 (10.8, 4.5)	–	–	T5-1	7.3 (8.3, 6.3)	–	11.2 (13.6, 8.8)
194	12.8 (17. 9.6)	2.4 (2.9, 1.9)	0.41 (0.49, 0.30)	T5-2	10.2 (13.9, 6.5)	–	–
Series 4: 1250 °C, MHO buffer, variable Cr_2O_3				T5-3	10.2 (14.7, 5.7)	–	–
189	7.6 (9.4, 6.3)	1.1 (1.3, 0.9)	0.35 (0.36, 0.30)	T5-4	–	4.1 (4.8, 3.4)	8.8 (10.6, 7.0)
201	8.0 (9.7, 6.7)	1.9 (2.3, 1.5)	0.11 (0.13, 0.09)	T5-5	5.0 (5.9, 4.1)	4.0 (4.9, 3.1)	11.5 (13.9, 9.1)
202	5.0 (6.6, 3.7)	1.2 (1.5, 0.9)	0.12 (0.15, 0.10)				
				T11-1	6.3 (7.4, 5.2)	–	6.3 (7.6, 5.0)
				T11-2	9.5 (12.2, 6.8)	–	–
				T11-3	8.4 (12.4, 4.4)	2.6 (2.9, 2.3)	8.8 (10.6, 7.0)
				T11-4	4.3 (5.2, 3.4)	3.6 (4.5, 2.7)	8.1 (9.8, 6.4)
				T11-5	4.9 (5.8, 4.0)	3.5 (4.2, 2.8)	8.0 (9.7, 6.3)
				T14-1	2.9 (4.8, 1.0)	–	16.7 (20.2, 13.2)
				T14-2	25.7 (29.3, 22.1)	5.8 (6.9, 4.7)	3.2 (3.9, 2.5)
				T14-3	17.0 (18.4, 15.6)	3.4 (4.8, 2.0)	4.3 (5.2, 3.4)
				T14-4	10.3 (12.7, 7.9)	6.8 (7.2, 6.4)	2.3 (2.8, 1.8)
				T14-5	4.0 (5.3, 2.7)	5.9 (6.2, 5.6)	3.6 (4.4, 2.8)

Numbers in parentheses represent the high and low values of the partition coefficient, according to the uncertainties on the spinel and glass analyses.
[a] Indicates anomalous values (see text) that we ignore as suspicious.

tetrahedral sites, and "inverse" if it occupies the tetrahedral sites and half of the octahedral sites. Crystal field stabilization energy, ionic radii, and valence all determine the location of cations in the structure. For the major elements in natural spinels, octahedral site preference energies probably decrease in the order $Cr^{3+} > Al^{3+} > Ti^{4+} > Fe^{2+}$ (Papike et al., 2005), so that trivalent and tetravalent cations are generally found in octahedrally coordinated B sites, and divalent cations in either the A or B sites. The structural transformation from "normal" to "inverse" in the spinel solid solution series must accommodate the charge balance requirements of the oxygen ligands: an oxygen (2−) must receive a 2+ charge from three octahedral cations and one tetrahedral cation (e.g., Papike et al., 2005).

4.1. Equilibrium considerations

Equilibrium between spinel and silicate melt can be assessed by examining the distribution of key major

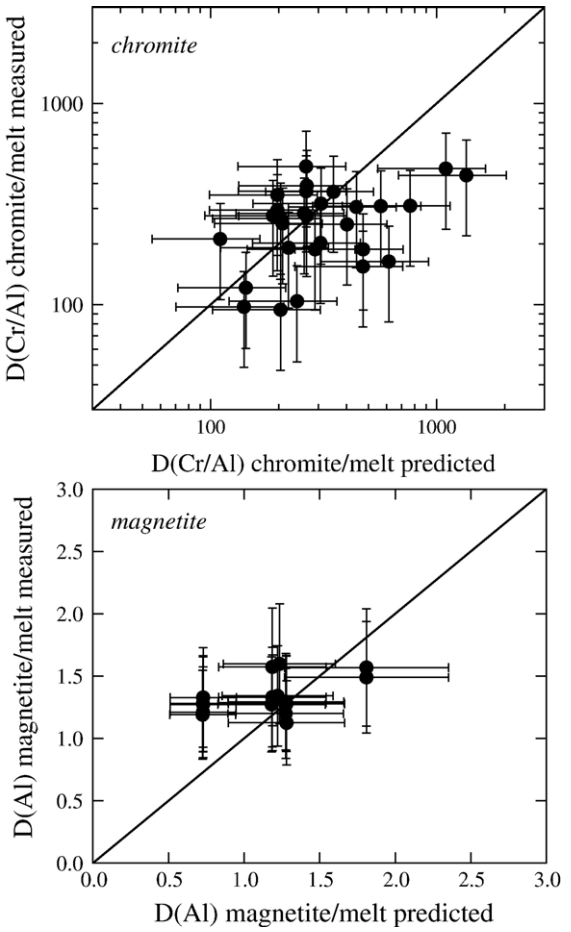

Fig. 6. Comparison of measured vs. predicted D(Cr/Al) chromite/melt and D(Al) magnetite/melt for new runs. Predicted values are from the studies of Ariskin and Barmina (1999) and Ariskin and Nikolaev (1996).

elements between both phases. Compositions of co-existing silicate melt and spinel have been studied extensively by Ariskin and Barmina (1999) and Ariskin and Nikolaev (1996), who have derived empirical expressions for partitioning of major elements as a function of T, fO_2 and melt composition. For those experiments containing magnetite-rich spinels, we have used the equilibrium partitioning of Al between spinel and melt and the expression:

$$\ln D(\mathrm{Al}) = a/T + b\log fO_2 + c + d_1X_{\mathrm{Na}} + d_2X_{\mathrm{K}} + d_3X_{\mathrm{P}}$$

where a, b, c and d_1–d_3 are from Ariskin and Barmina (1999). For those experiments containing chromian-rich spinels, we have used the equilibrium partitioning of Cr/Al between spinel and melt and the expression:

$$\ln D(\mathrm{Cr/Al}) = a/T + b\log fO_2 + c\ln\left(\mathrm{Fe^{3+}/Fe^{2+}}\right)\mathrm{liq} + d(\mathrm{NBO}/T) + e$$

where a–e are from Ariskin and Nikolaev (1996) and NBO/T is calculated according to Mysen (1991). Comparison of calculated and measured D(Al) and D(Cr/Al) for experiments reported in Table 2 (Fig. 6) shows good agreement, and suggests that equilibrium was approached in these runs. Additional evidence for an approach to equilibrium in these experiments is the presence of homogeneous, unzoned spinels. Spinels produced in most experiments were unzoned from core to rim in terms of FeO, Cr_2O_3, MgO and other elements. A few spinels that were slightly zoned (e.g., 15.4% in core to 8.4% in rim for Cr_2O_3 in run 191) were also included in this study, as such slight zoning apparently had only a minimal effect on partitioning of Ni, Co and V since D for these elements are indistinguishable from those from other runs at similar conditions.

Approach to equilibrium can also be monitored by use of the olivine–liquid equilibrium:

$$\underset{\text{(liquid)}}{2\mathrm{FeO}} + \underset{\text{(olivine)}}{\mathrm{Mg_2SiO_4}} = \underset{\text{(liquid)}}{2\mathrm{MgO}} + \underset{\text{(olivine)}}{\mathrm{Fe_2SiO_4}}\,. \qquad (1)$$

Olivine compositions produced in a subset of the new runs and in all of those of Leeman (1974) (see Table 2) are in good agreement with the compositions predicted by the method of Snyder and Carmichael (1992). For these calculations, X_{FeO} in the silicate liquid was calculated from run temperature and oxygen fugacity using the expression in Kress and Carmichael (1991). In addition, Cr_2O_3 contents of glasses produced in these runs are <0.2 wt.%, as expected for melts in equilibrium with Cr-rich spinels at 1200–1300 °C and oxygen fugacities higher than the QFM buffer (Roeder and Reynolds, 1991).

Series 1 runs and run #183 (Series 2) were done with Ni–NiO and Co–CoO buffers enclosed with the sample.

Fig. 7. (A) Variation of D(Ni) spinel/melt with X_{Ni} for spinels from this study (Series 1 to 4 and T experiments), as well as results from previous studies of Lindstrom (1976), Nielsen et al. (1994), Horn et al. (1994) and Toplis and Corgne (2002). Symbols for previous studies are slightly smaller than those for the new results. Note anomalously high value for experiment 190. (B) Variation of D(Co) spinel/melt with X_{Co} for spinels from this study (Series 1 to 4 and T experiments), as well as results from previous studies of Lindstrom (1976), Horn et al. (1994) and Toplis and Corgne (2002). Symbols for previous studies are slightly smaller than those for the new results. Note anomalously high value for experiment 196. (C) Variation D(V) spinel/melt with X_{V} for spinels from this study (Series 1 to 4 and T experiments), as well as results from previous studies of Lindstrom (1976), Nielsen et al. (1994), Horn et al. (1994), Canil (1997, 2002) and Toplis and Corgne (2002). Symbols for previous studies are slightly smaller than those for the new results.

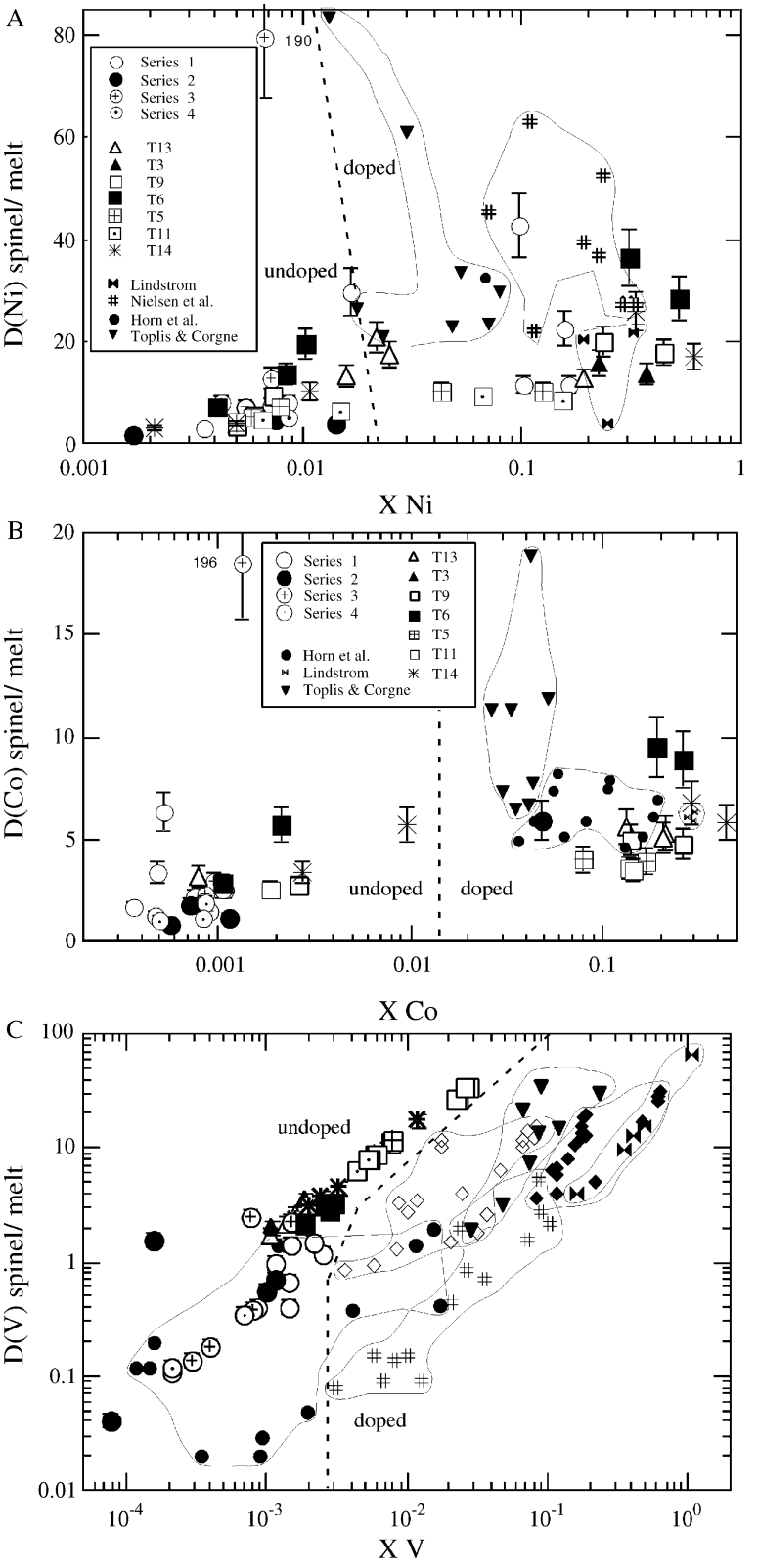
A
D(Ni) spinel/ melt
X Ni
190
doped
undoped
Series 1
Series 2
Series 3
Series 4
T13
T3
T9
T6
T5
T11
T14
Lindstrom
Nielsen et al.
Horn et al.
Toplis & Corgne
B
D(Co) spinel/ melt
X Co
196
undoped
doped
C
D(V) spinel/ melt
X V
undoped
doped

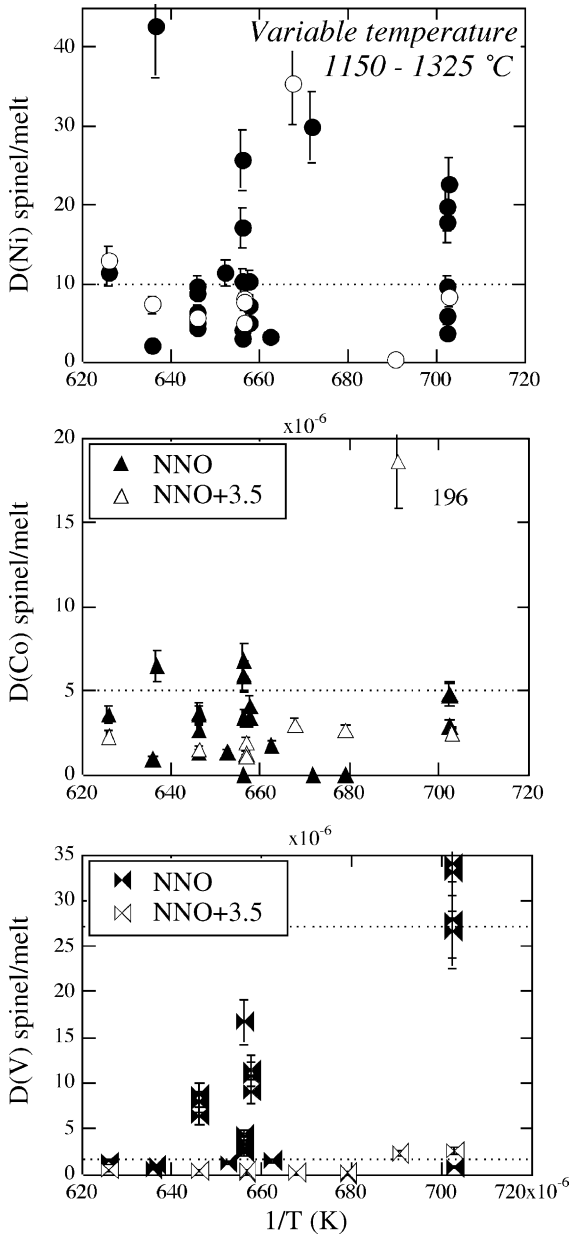

Fig. 8. D(Ni), D(Co) and D(V) spinel/melt vs. $1/T$ (K) for experiments carried out near the NNO buffer (solid symbols, ± 1 log fO_2 unit from NNO buffer) or at NNO+3.5 (open symbols), but at temperatures between 1150 and 1325 °C. No systematic effect of temperature is evident in this dataset. Such effects may be subtle and masked by larger compositional effects. Horizontal dashed lines indicate the D(Ni) and D(Co) values used in later modeling. Note anomalously high value for experiment 196.

Although original basaltic powder contained only natural levels of Ni and Co, the run products were enriched in Ni or Co, clearly indicating an exchange of Ni and Co between the buffer and sample. Because the results from these experiments also show some scatter (e.g., Fig. 7) compared to the other series and runs of Leeman (1974), the results should be interpreted with caution. Although it is likely that each experiment approached equilibrium, as discussed above, the high levels of Ni or Co make interpretation and comparison with other runs more complicated. Runs 190 and 196 are clearly anomalous for Ni and Co, respectively. In each case, glass analyses are unusually low, resulting in very high spinel partition coefficients. Accordingly, these runs are ignored in discussions of our data.

Comparison of our results to those of previous studies using doped compositions reveals that the partition coefficients in doped runs are often higher (Fig. 7). An important feature of most data sets is that the spinel–melt partition coefficients increase with increasing concentration of Ni, Co or V in spinel, even when temperature and relative oxygen fugacity are nearly constant (Fig. 7). In addition, D(V) spinel/melt varies with compositional parameters such as X_{Ti} and X_V. Because Ni and Co exhibit distinct behavior from V, they will be discussed separately below.

4.2. Spinel/melt partition coefficient

4.2.1. Nickel and cobalt

Temperature, oxygen fugacity and composition are the main factors thought to influence partitioning behavior, and each will be addressed below.

Two sets of experiments can be examined for potential temperature effects at NNO and at MHO, with each series including data from experiments carried out between 1150 and 1325 °C. It is clear from both series that there is no systematic variation of either D(Ni) or D(Co) spinel/melt attributable to temperature alone (Fig. 8). Variation in both series is more likely related to differences in spinel composition, as will be seen below.

Table 11
Comparative spinel structures and unit cells (from Hill et al., 1979)

Spinel	Unit cell (Å)
$MgAl_2O_4$	8.0832
$FeAl_2O_4$	8.149
$MgCr_2O_4$	8.333
Fe_2TiO_4	8.392
Mg_2TiO_4	8.445
MgV_2O_4	8.530
$NiAl_2O_4$	8.043
$NiCr_2O_4$	8.305
$NiFe_2O_4$	8.325
$CoAl_2O_4$	8.095
$CoCr_2O_4$	8.332
$CoFe_2O_4$	8.350

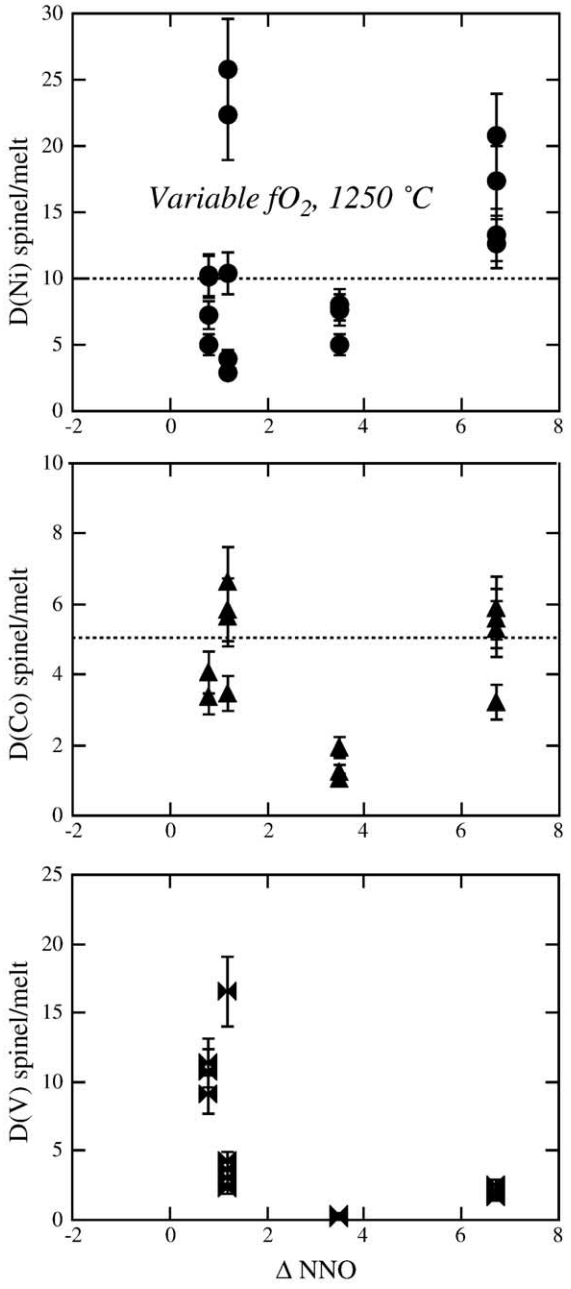

Fig. 9. D(Ni), D(Co) and D(V) spinel/melt vs. ΔNNO for experiments carried out at 1250 °C. No systematic effect of oxygen fugacity is evident in this dataset. Variation in some of the partition coefficients is due instead to differences in composition (Ti-bearing vs. T-free spinel) or doping levels. Horizontal dashed lines indicate the D(Ni) and D(Co) values used in later modeling.

Because Ni and Co are divalent across a wide range of oxygen fugacity that cover the range of our study (Capobianco and Amelin, 1994; Holzheid and Palme, 1996), any variation in D(Ni) or D(Co) spinel melt cannot be attributed to a change in valence. However, the effect of variable fO_2 may change the composition of spinel that crystallizes from a basaltic liquid (e.g., Horn et al., 1994). Thus, variation in D(Ni) or D(Co) spinel/melt could be due to structural changes in the spinel as a consequence of extensive solid solution that is possible between Cr-, Ti-, Al- and Fe^{3+}-end members, as well as Ni-, Co- and V-rich end members (e.g., see the variation

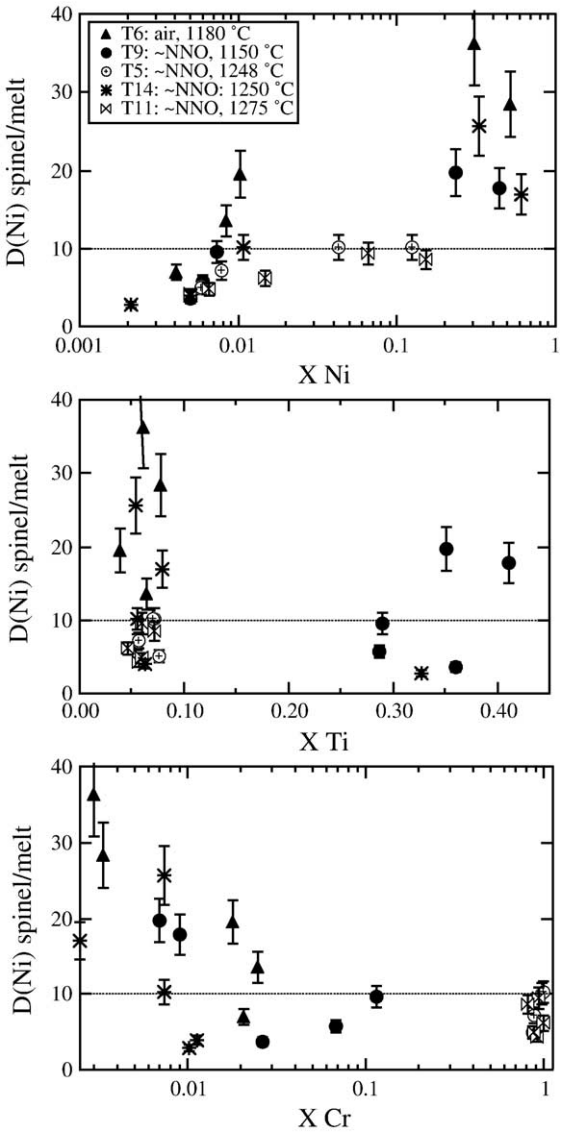

Fig. 10. Variation in D(Ni) spinel/melt with X_{Ni}, X_{Ti} and X_{Cr} of spinels from series T9, T6, T5, T11 and T14. Within each series, five experiments were done at fixed temperature and oxygen fugacity, but variable dopant level. Because T and fO_2 are constant, these figures illustrate the effect of changing the bulk Ni content of the system on the magnitude of the partition coefficient. Horizontal dashed lines indicate the D values used in later modeling. Experiments T13 and T3 are omitted for clarity; their D values are in the range of the data shown.

in unit cell in various spinels; Table 11). A series of experiments carried out at 1250 °C and across 7 orders of magnitude change in oxygen fugacity reveals no clear dependence upon oxygen fugacity considering the variability of D values within each experiment (Fig. 9). The direct effect of changing oxygen fugacity is likely to be small, as suggested by the data of Toplis and Corgne (2002) for magnetite/melt partitioning of Ni, Co and Mn. Thus, the differences in D(Ni) and D(Co) spinel/melt observed between runs in Fig. 9 are most likely related to changes in spinel composition.

There are not clear variations in D with changing major element composition (Al, Cr, Ti, Fe^{3+}), but there are some variations that are related to Ni or Co content. Although there may be a slightly higher D(Ni) observed in some Ti- or Fe^{3+}-bearing spinels (Fig. 10), there are many Ti-rich spinels for which D(Ni) are low. Similarly, Cr-bearing spinels exhibit both low and high D(Ni) and D(Co) values (Figs. 5 and 6), indicating that Cr content is not a dominant controlling factor in the value of the partition coefficient. The most significant factor in many data sets appears to be the Ni or Co content of the spinel (Figs. 10 and 11). For instance, the highest D's in individual data sets are generally those in which the spinels have the highest Ni and Co content (Figs. 7 10 and 11), but similar major element bulk compositions (e.g., Cr, Al, Ti, Fe^{3+}). In particular, the runs of Leeman (1974) show increasing D(Ni) and D(Co) with Ni and Co content. Because some of these spinels are very Ni- and Co-rich, the unit cell sizes will be larger than most natural spinels (Table 11), and this may have a large effect on the partition and activity coefficients. In summary, variations in D(Ni) and D(Co) spinel/melt are likely a result of spinel compositional variation. Spinels with lower Ni or Co contents generally yield lower partition coefficients, suggesting that previous experimental studies involving doped systems, have overestimated partition coefficients.

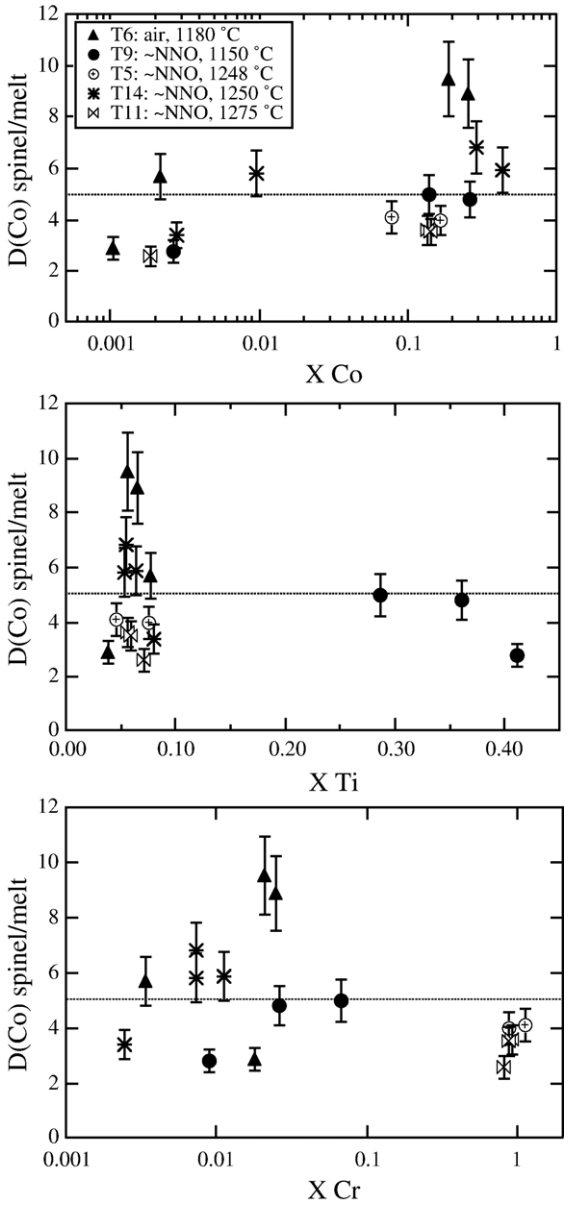

Fig. 11. Variation in D(Co) spinel/melt with X_{Co}, X_{Ti} and X_{Cr} of spinels from series T9, T6, T5, T11 and T14. Within each series, five experiments were done at fixed temperature and oxygen fugacity, but variable dopant level. Because T and fO_2 are constant, these figures illustrate the effect of changing the bulk Co content of the system on the magnitude of the partition coefficient. Horizontal dashed lines indicate the D values used in later modeling. Experiments T13 and T3 are omitted for clarity; their D values are in the range of the data shown.

4.2.2. Vanadium

Unravelling the controlling variables behind partitioning of V in spinels has proven difficult because temperature, oxygen fugacity, and spinel chemistry are linked and difficult to separate experimentally. As with Ni and Co, variation in D(V) spinel/melt may be a result of variation in all three of these parameters.

The influence of temperature has been difficult to isolate due to use of different bulk compositions and oxygen fugacities in experimental studies. Variation in D(V) spinel/melt in suites at constant fO_2 (the most reduced runs, near NNO; Fig. 8), but variable temperature, suggest some dependence upon temperature (Fig. 8). However, some of the variation seen in Fig. 8 can be attributed (as will be seen below) to compositional differences in the spinel (e.g., high and low Ti spinels at the same fO_2). If one focuses instead on systems of similar composition and constant fO_2, there are clear

differences in D(V) that can be attributed to temperature; specifically, D(V) increases at lower temperatures (Fig. 8). It is also interesting to note that the higher oxygen fugacity runs do not show any temperature dependence, perhaps due to the stability of V^{5+}, which is likely to be incompatible in spinel regardless of temperature.

Variation in D(V) arising from changing oxygen fugacity is likely to be extensive, because V is multivalent, stable in 5+, 4+, 3+ under terrestrial conditions and perhaps 2+ under highly reducing conditions (Borisov et al., 1987; Schreiber et al., 1987; Delaney et al., 2002). Evidence that V^{3+} is likely to be compatible in spinels comes from both natural and experimental systems. The negative correlation between Cr and V and the positive correlation between Ti and V observed in terrestrial spinels may imply that V is predominantly trivalent and entering spinel on the octahedral site like Cr (e.g., Nehru et al., 1974). An Al–V anti-correlation ob-

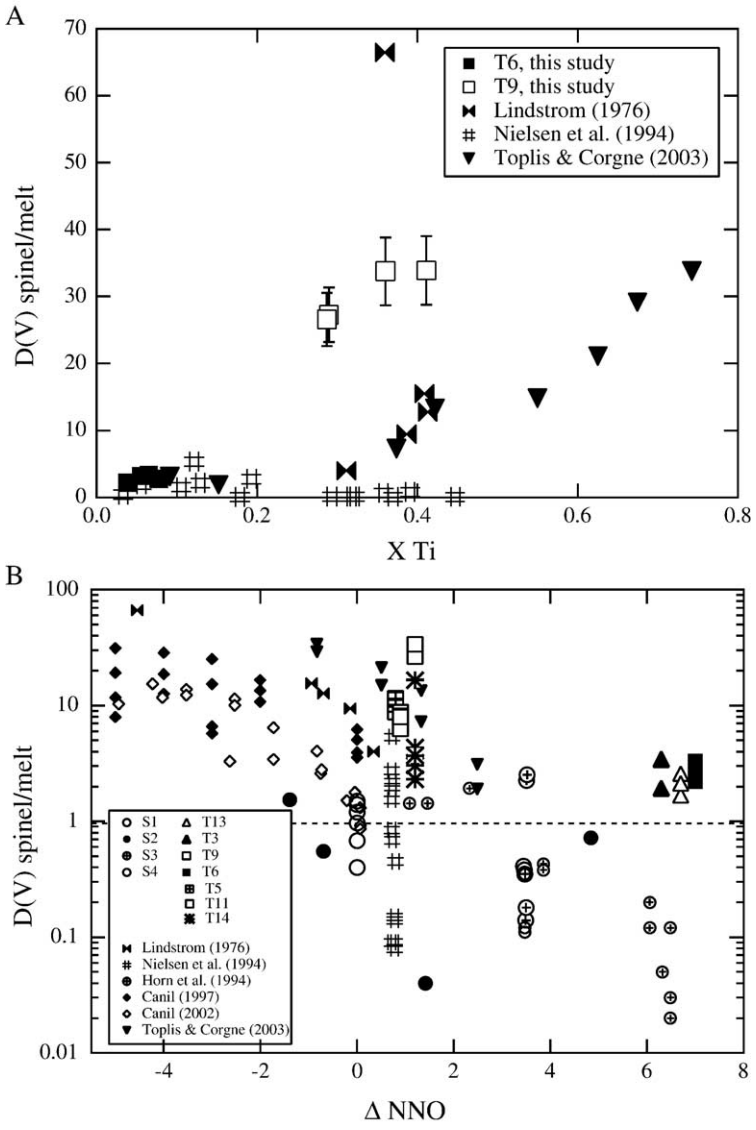

Fig. 12. D(V) spinel/melt vs. X_{Ti} and fO_2, illustrating the importance (and interdependence) of these variables. (A) The strong effect of X_{Ti} on D(V) spinel/melt is illustrated in three different data sets—our experiment T9, Lindstrom (1976) and Toplis and Corgne (2002). (B) Although there is an overall dependence of D(V) spinel/melt on fO_2, as suggested in several previous studies, this effect is accompanied by variation due to temperature and compositional effects. Consideration of all data together makes such D(V)–fO_2 correlations less coherent. To understand the cause of variation in D(V) spinel/melt completely will require an understanding of each of these variables separately and independently of one another. Symbols for previous studies are slightly smaller than those for the new results.

served in experimentally produced aluminous spinels (Mg–V–Al–O system) provides further evidence for trivalent V substitution (Canil, 2002). It has been recognized that D(V) is dependent upon oxygen fugacity (Lindstrom, 1976; Horn et al., 1994; Toplis and Corgne, 2002; Figs. 9 and 12), but when all data are considered together it is evident that scatter in the trend must be due to the additional effects of temperature and spinel composition (Fig. 9).

There is also a strong spinel compositional control on D(V), with V and TiO_2 contents of spinel being most important (Figs. 7 and 12). For example, four different series at nearly constant fO_2 from the Leeman (1974) runs show a positive correlation of D(V) with TiO_2 and V, but also a significant temperature-dependence (Fig. 13). In addition, series T14 shows that high TiO_2 spinel (in run #14-1) will cause a higher D(V) at constant T, fO_2 and V doping level (Fig. 13). Cr_2O_3 content of spinel, on the other hand, appears to have relatively little influence on D(V); Cr_2O_3-bearing spinels produced near the NNO buffer define the same range of D(V) as those that are Cr_2O_3-poor (Figs. 7 10 and 13).

Finally, the effect of composition and oxygen fugacity is sometimes combined. For example, for four different runs of Leeman (1974) at variable fO_2, but

Table 12
Regression parameters for D(V)

Term	Constant	Value	Standard error
$1/T$	a	−9695	6770
Log fO_2	b	−0.288	0.065
X_{Cr}	c	5.10	4.92
X_{Fe3+}	d	2.65	4.82
X_{Al}	e	−0.20	4.91
X_{Ti}	f	6.33	5.14
V in glass (ppm)	g	4.38×10^{-6}	3.64×10^{-6}
Mg#	h	−2.35	0.79
	i	3.84	7.23

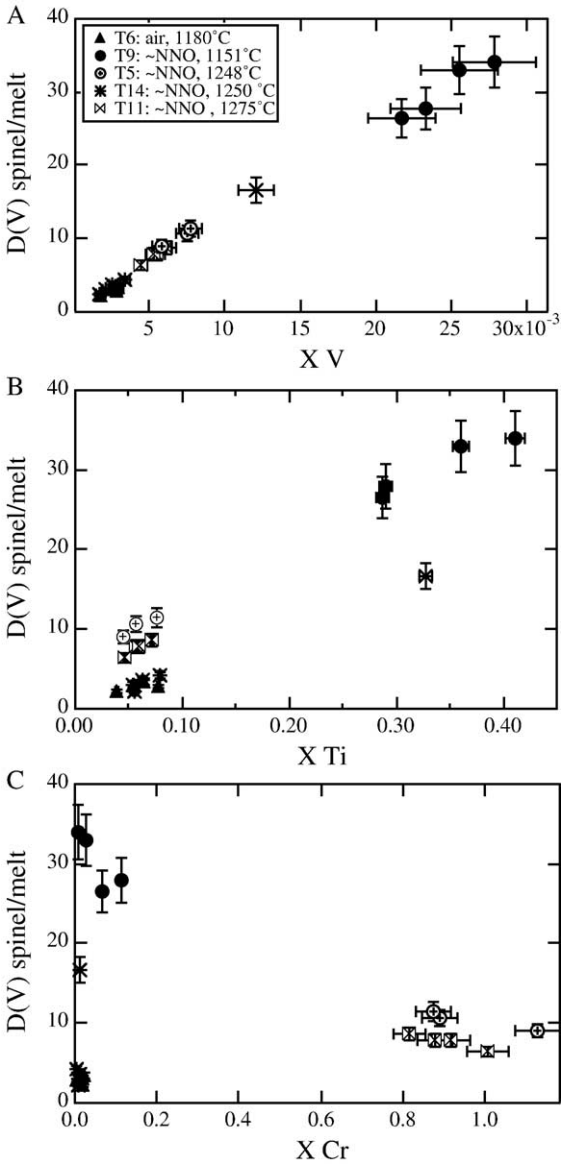

Fig. 13. Variation in D(V) spinel/melt with X_V, X_{Ti} and X_{Cr} of spinels from series T9, T6, T5, T11 and T14. Within each series, five experiments were done at fixed temperature and oxygen fugacity, but variable dopant level. Because T and fO_2 are constant, these figures illustrate the effect of changing the bulk V content of the system on the magnitude of the partition coefficient and also illustrate the strong effect of X_{Ti} on D(V). Experiments T13 and T3 are omitted for clarity; their D values are in the range of the data shown.

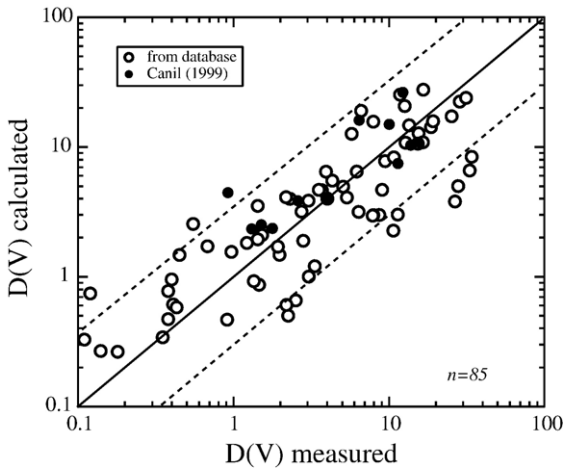

Fig. 14. Comparison of D(V) spinel/melt measured and D(V) spinel/melt calculated using Eq. (2) and the regression constants from Table 10. Dashed line indicates a perfect 1:1 correlation; the experimental data were taken from this study and from published experiments (Lindstrom, 1976; Horn et al., 1994; Nielsen et al., 1994; Canil, 1997).

constant temperature (1250 °C), D(V) increases at lower fO_2. However, because some of the lower fO_2 runs contain spinels with higher TiO_2 contents, it is difficult to know whether the variation in D(V) is due to TiO_2 content or to fO_2, or both, because the TiO_2 content of the spinel is also dependent upon fO_2. Insight into the actual controls may come from further experiments at near constant temperature and oxygen fugacity, but variable TiO_2 content (Fig. 7).

Many previous studies done at reduced conditions have reported compatibility of V in spinel-structured oxides, but many of the spinels have V_2O_3 contents >1 wt.% and some have as much as 25 to 40 wt.% (Lindstrom, 1976; Nielsen et al., 1994; Canil, 2002). Can the variation observed in D(V) be due to non-Henrian behavior of V partitioning between spinel and silicate melt? Although there is a clear correlation between D(V) and V content of spinels (Figs. 7 10 and 13), such a conclusion may be premature. First, the Horn et al. (1994) data show no systematic dependence upon V content (albeit over a small compositional range), suggesting that Henrian behavior is observed. Second, the D(V) range determined in this study for undoped experiments is similar to the D(V) range defined by doped experiments at similar temperatures and oxygen fugacities by Canil (2002) and Toplis and Corgne (2002).

In order to predict D(V) as a function of temperature, oxygen fugacity and spinel composition, we have undertaken multiple linear regression on a total of 85 experiments analyzed in this study, as well as from Lindstrom (1976), Canil (1997), Nielsen et al. (1994) and Horn et al. (1994). Experiments done at the most oxidizing conditions (air) were

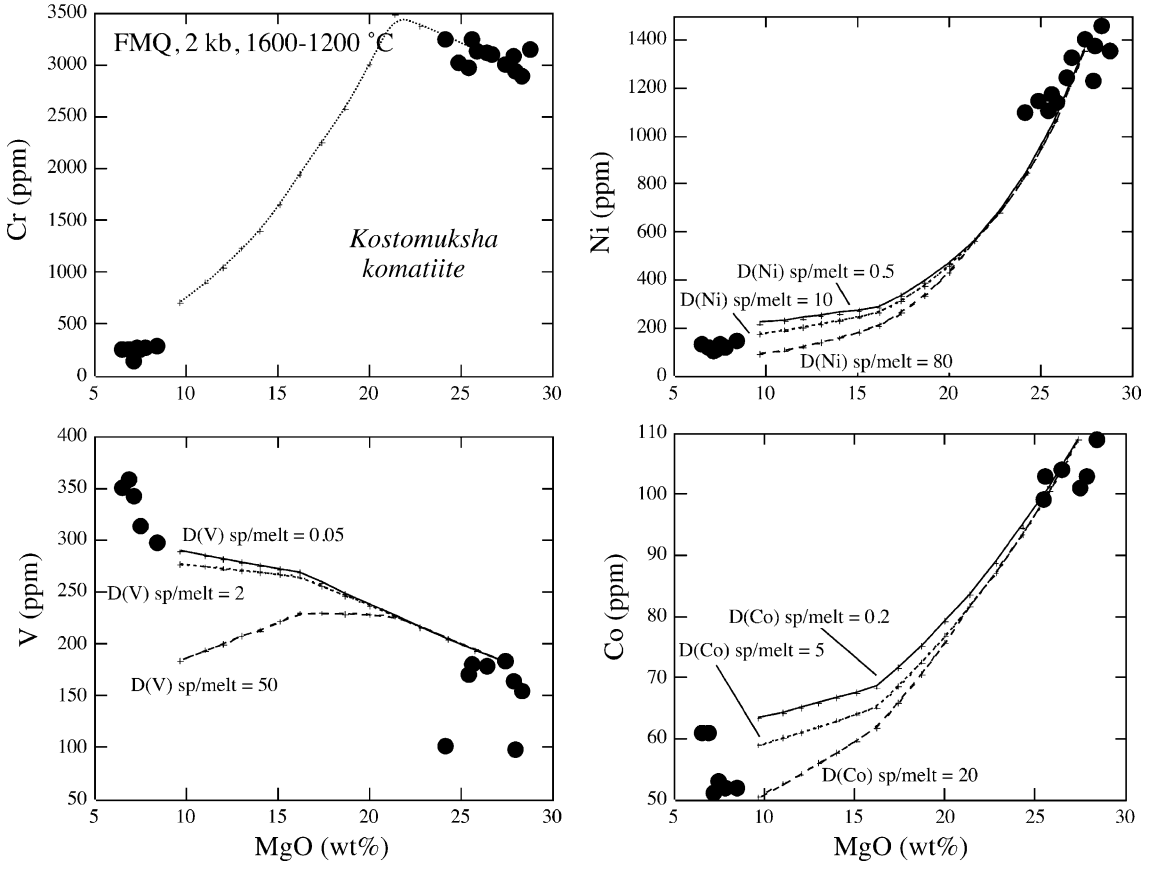

Fig. 15. MgO (wt.%) vs. Cr, Ni, Co and V (all ppm) for the Kostomuksha komatiite suite. Major element modelling of crystal fractionation of the proposed Kostomuksha parent liquid (Puchtel and Humayun, 2000; Puchtel et al., 1998) was carried out using the MELTS program (Ghiorso and Sack, 1994) from 1600 to 1200 °C, at 2 kb and the QFM oxygen buffer. Crosses indicate the calculated trends using the major element results (at 25 °C intervals). The amount of olivine fractionated before chromite saturation is 20.5% and the amount after is 32.9%. Trace element concentrations are calculated using the results of this study (for spinel) and published D's of Green (1994) and Roeder and Reynolds (1991): D(Ni): olivine/melt=5, spinel/melt=10, opx/melt=1, cpx/melt=1; D(Co): olivine/melt=2.3, spinel/melt=5, opx/melt=1, cpx/melt=1; D(V): olivine/melt=0.01, spinel/melt=14, opx/melt=0.5, cpx/melt=0.5; D(Cr): olivine/melt=0.36, spinel/melt=220, opx/melt=0.1, cpx/melt=0.1.

left out of the regression analysis, since application of the results will be made to samples that equilibrated at more reducing conditions between the HM and IW buffers. Because all four spinel end members–Ti-, Al-, Cr- and Fe^{3+}-bearing–are potentially important in controlling D(V), we have included terms for each in the linear regression. The equation is of the form:

$$D(\mathrm{V}) = a(1/T) + b(\log fO_2) + c(X_{\mathrm{Cr}}) + d\left(X_{\mathrm{Fe}}^{3+}\right) + e(X_{\mathrm{Al}}) + f(X_{\mathrm{Ti}}) + g(\mathrm{V\ in\ glass}) + h(\mathrm{Mg\#\ spinel}) + i \quad (2)$$

where constants a through i are calculated and presented in Table 12. Comparison of measured and calculated values (Fig. 14) shows that this expression recaptures the input data well. Also shown are the results from Canil (1999) which were calculated using Eq. (2) and compared to their measured values. Since they are not included in the input database for deriving the regression constants, it demonstrates that the expression effectively captures variation in D(V) due to temperature, composition and oxygen fugacity.

5. Application of results to terrestrial magmatic suites

An alternative way to evaluate transition metal partitioning in spinels is to invert compositions of cogenetic magma suites for which spinel is a liquidus phase (cf. Leeman et al., 1978). Here we follow this approach considering several well characterized natural magmatic suites: komatiites (Puchtel et al., 1998; Puchtel and Humayun, 2000), MORB (mid-ocean ridge basalt; Schilling et al., 1983), Hawaiian lavas (HSDP; Hawaiian Scientific Drilling Program; Rhodes, 1996; Albarède, 1996), a basalt to latite series from Craters of the Moon (Leeman et al., 1976), and a basalt to rhyolite series from Volcan Alcedo, Galapagos Islands (Geist et al., 1995). In each of the cases below, parent liquids were selected from the individual studies and major element liquid lines of descent calculated using the MELTS computer program (Ghiorso and Sack, 1994). Because the amount of spinel crystallization is sensitive to subtle changes in melt Cr content, and this is not modeled well using the MELTS program, Cr contents were estimated using D(Cr) spinel/melt values based on

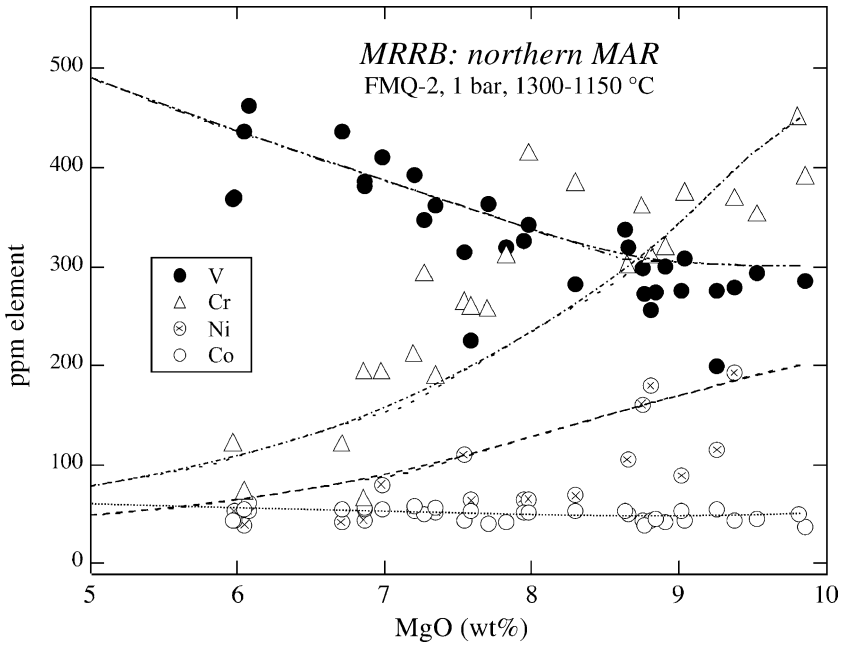

Fig. 16. Correlations between Ni, Co, V and MgO within a MORB suite from the northern mid-Atlantic ridge (Schilling et al., 1983). Schilling et al. (1983) report fewer Ni data than for the other elements. Major element modelling was carried out using the MELTS program (Ghiorso and Sack, 1994) from 1300 to 1150 °C, at 1 bar and 2 log fO_2 units below the QFM oxygen buffer. Crosses indicate the calculated trends using the major element results (at 25 °C intervals). Calculated trends (using major element modeling) use spinel/melt partition coefficient data from this study and partition coefficients for olivine from Green (1994). The variation can be ascribed to progressive liquid evolution during fractionation of 0.6% chromite, 8.4% olivine, 26.0% feldspar and 22.9% pyroxene. Trace element concentrations are calculated using the results of this study (for spinel) and published D's of Green (1994) and Roeder and Reynolds (1991): D(Ni): olivine/melt=5, spinel/melt=10, cpx/melt=1; plag/melt=0.001; D(Co): olivine/melt=2, spinel/melt=5, cpx/melt=1, plag/melt=0.001; D(V): olivine/melt=0.1, spinel/melt=14, cpx/melt=0.5, plag/melt=0.001; D(Cr): olivine/melt=0.5, spinel/melt=150, and cpx/melt=1, plag/melt=0.01.

the work of Roeder and Reynolds (1991). The MELTS results (solid and liquid compositions) and the D(Cr) modelling were then coupled with partition coefficient data for Ni, Co and V (from this study for spinel and from the literature for olivine, pyroxenes and feldspar). Because the komatiite, MORB and HSDP suites are basic liquids that evolved near the QFM buffer, values of D(Ni) spinel/melt=10, D(Co) spinel/melt=5. D(V) spinel/melt was calculated for each suite, using the spinel composition predicted by the MELTS program, V content of the liquid, temperature and fO_2 and Eq. (2). It should be emphasized that these models are not unique. The calculations and modeling presented here are meant to be illustrative, and a range of D(Ni), D(Co), D(V) as well as T, P, fO_2 and composition could reproduce the data.

5.1. Komatiites

The Kostomuksha komatiite suite has been studied in detail by Puchtel et al. (1998) and Puchtel and Humayun (2000). The variation in major elements and Cr can be understood by fractionation of olivine and chromite from a MgO-rich parent liquid. This variation has been modeled specifically, using the MELTS program at conditions of 1600 to 1200 °C and 200 MPa at the QFM oxygen buffer (Fig. 15). The amount of olivine fractionated before chromite saturation is 20.5% and the amount after is 32.9%. Because this suite is well understood and fractionation of only olivine and chromite can account for the variation, this suite was chosen to illustrate the sensitivity of the modelling to chosen values of D(Ni) spinel/melt, D(Co) spinel/melt and D(V) spinel/melt. The effect of using a range of values for D(Ni), D(Co) and D(V) spinel/melt is demonstrated (Fig. 15), while the proportion of fractionated olivine and chromite, as well as the olivine/melt partition coefficients for Ni, Co and V, are kept constant. It is clear that D(Ni) spinel/melt=10, D(Co) spinel/melt=5 and D(V) spinel/melt=14 (calculated using Eq. (2)) can adequately explain the trends for Ni, Co and V with MgO.

5.2. MORB

Major and minor element (including MgO and Cr) trends in a suite of basalts from the northern Mid-Atlantic Ridge can be ascribed to progressive liquid

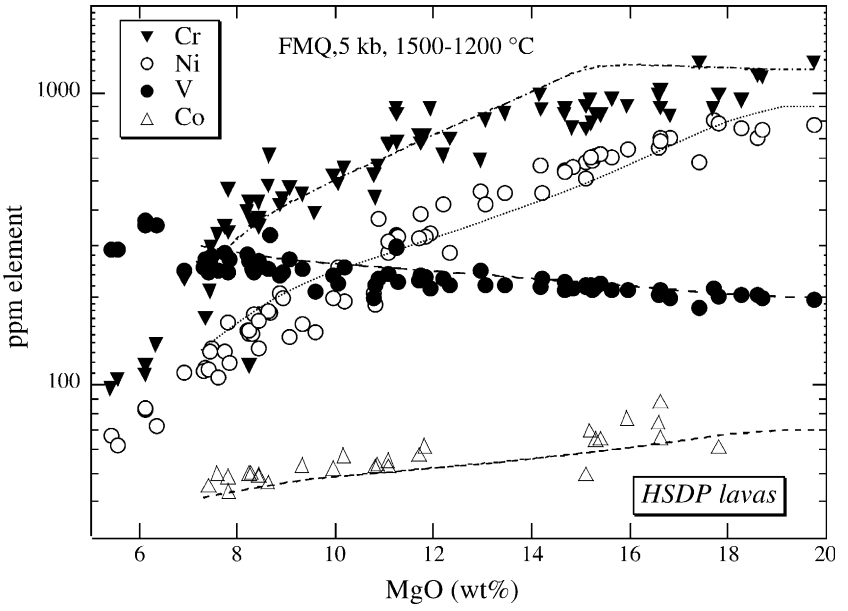

Fig. 17. Correlations between Ni, Co, Cr, V and MgO among Mauna Kea lavas from the Hawaiian Scientific Drilling Project (HSDP) suite (Rhodes, 1996; Albarède, 1996). The calculated trends are those resulting from major element modeling using MELTS (Ghiorso and Sack, 1994), and assuming sample R091 as a parental liquid at 5 kb, QFM buffer, between 1500 and 1200 °C. The trends shown correspond to liquid evolution during fractionation of 11.6% olivine, 34.3% orthopyroxene and 0.53% spinel. Trace element concentrations are calculated using the results of this study (for spinel) and published D's of Green (1994) and Roeder and Reynolds (1991): D(Ni) spinel/melt=10, D(Ni) olivine/melt=6, D(Ni) orthopyroxene/melt=3, D(Co) spinel/melt=5, D(Co) olivine/melt=2, D(Co) orthopyroxene/melt=1.5, D(V) spinel/melt=15, D(V) olivine/melt=0.1, D(V) orthopyroxene/melt=0.4, D(Cr) spinel/melt=150, D(Cr) olivine/melt=0.6 and D(Cr) orthopyroxene/melt=2. The Ni and Co spinel partition coefficients are the same as those use for modelling the Kostomuksha komatiite suite and also the mid-Atlantic Ridge basalts (Figs. 15 and 16).

evolution during fractionation of chromite, olivine, plagioclase feldspar and clinopyroxene; based on MELTS modeling, crystallization conditions appear to range from 1300 to 1150 °C, at 1 bar and 2 log fO_2 units below the QFM oxygen buffer. Notably, there is a trend of increasing V with decreasing Cr, Ni, Co and MgO (Fig. 16). At MORB-relevant oxygen fugacities (e.g., QFM; Christie et al., 1986), previous studies have indicated that D(V) spinel/melt is as high as 28 (Canil, 1997, 2002). Here, we calculate using Eq. (2) a value of 14, similar to values measured by Canil (1997, 2002). Using D(Ni) spinel/melt=10, D(Co) spinel/melt=5 and D(V) spinel/melt=14, fractionation of 0.6% chromite, 8.4% olivine, 26.0% feldspar and 22.9% pyroxene satisfactorily reproduces the MORB data.

5.3. OIB (Hawaii)

Lavas drilled from the flanks of Mauna Kea for the Hawaiian Scientific Drilling Project (HSDP) can be used to examine the behavior of Ni, Co and V in OIB-type basalt. These basalts are thought to have differentiated at low pressures with oxygen fugacities

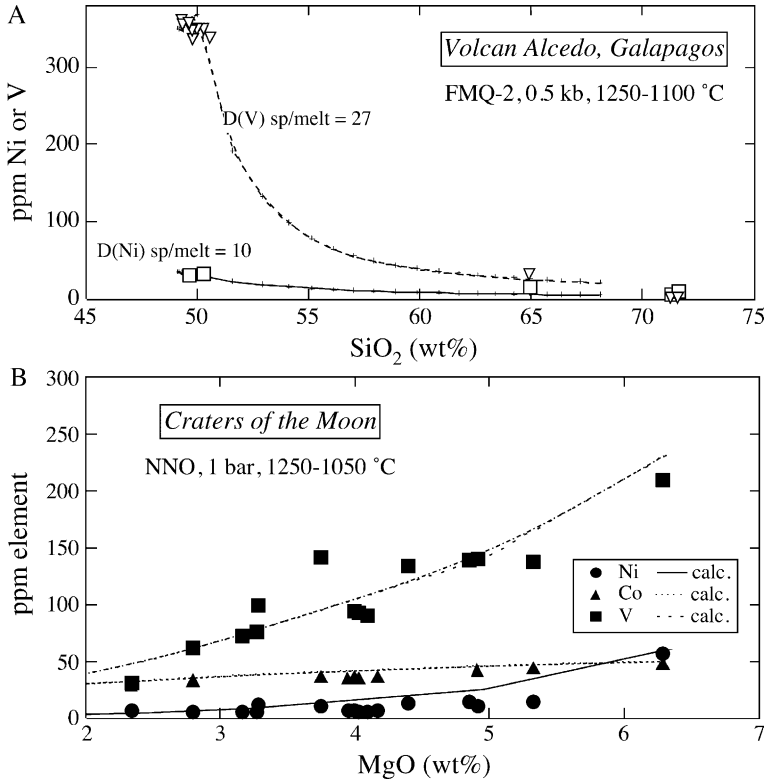

Fig. 18. (A) V and Ni variation with MgO for the Volcan Alcedo basalt to rhyolite suite (Geist et al., 1995). The variation can be adequately modelled using partition coefficients of D(V)=30 and D(Ni)=10. This spinel (magnetite) contains close to 15 wt.% TiO_2, similar to the spinel (magnetite) in the rhyolites (Geist et al., 1995). Solid lines with crosses are calculated liquid lines of descent for fractionation of DG30 basalt at 0.5 kb, FMQ-2, at 10 °C intervals (using MELTS of Ghiorso and Sack, 1994). Note the initial FeO–TiO_2 enrichment is due to the crystallization of olivine, augite and plagioclase. FeO and TiO_2 depletion is caused by the stabilization of magnetite among the fractionating phase assemblage. Both Ni and V decrease substantially once magnetite joins the fractionating assemblage, and can be modelled using the partition coefficients used in this study. The cumulative amount of phases fractionated is as follows: 11% olivine, 28% augite, 37% plagioclase and 6% magnetite. Trace element concentrations are calculated using the results of this study (for spinel) and published D's of Green (1994) and Roeder and Reynolds (1991): D(V): oliv/melt=1, cpx/melt=2, plag/melt=0.001, spinel/melt=30; D(Ni): oliv/melt=5, cpx/melt=1, plag/melt=0.001, spinel/melt=10. (B) Ni, Co and V variation with MgO in a suite of lavas from Craters of the Moon, Idaho (Leeman et al., 1976, 1978). The suites can be adequately modeled using the same set of partition coefficients as the Galapagos suite. The variation can be adequately modelled using partition coefficients of D(V) spinel/melt=26, D(Ni) spinel/melt=10 and D(Co) spinel/melt=5. Solid lines with crosses are calculated liquid lines of descent for fractionation of 69–28 basalt at 1 bar, NNO, at 20 °C intervals (using MELTS; Ghiorso and Sack, 1994). The cumulative amount of phases fractionated is as follows: 6% olivine, 13.3% augite, 34.9% plagioclase, 3.7% apatite and 16.3% magnetite. Trace element concentrations are calculated using the results of this study (for spinel) and published D's of Green (1994) and Roeder and Reynolds (1991): D(V): oliv/melt=1, cpx/melt=2, plag/melt=0.001, magnetite/melt=26 and apatite/melt=0.01; D(Ni): oliv/melt=5, cpx/melt=1, plag/melt=0.001, magnetite/melt=10 and apatite/melt=0.01; D(Co): oliv/melt=2, cpx/melt=2, plag/melt=0.01, magnetite/melt=5 and apatite/melt=0.01.

buffered near QFM (Baker et al., 1996). Chromium, Ni and Co all show decreasing concentrations with decreasing MgO, consistent with olivine- and spinel-control (Rhodes, 1996; Albarède, 1996; Fig. 17). However, V shows an inverse correlation with MgO and Cr, indicating its incompatibility (bulk $D<1$) during differentiation (Fig. 17). The concentrations of Ni, Cr, Co and V in this suite can be approximated using a fractional crystallization model with D(Ni) spinel/melt=10, D(Co) spinel/melt=5, D(V) spinel/melt=15 (calculated using Eq. (2)), and fractionation of 0.53% chromite, 11.6% olivine and 34.3% low Ca pyroxene from a parental liquid at 5 kb, QFM buffer, between 1500 and 1200 °C (using MELTS).

5.4. Volcan Alcedo (Galapagos) and Craters of the Moon (Idaho)

The basalt to rhyolite suite at Volcan Alcedo, Galapagos Islands (Geist et al., 1995) is thought to have formed by nearly pure fractional crystallization of olivine, pyroxene, plagioclase and titano-magnetite. Because magnetite appears late in the sequence and is different in composition from the Cr-bearing spinels modeled in other suites, we use this example to illustrate the effect of spinel composition on D(V). For Alcedo, the initial FeO–TiO_2 enrichment is due to the crystallization of olivine, augite and plagioclase, and later FeO and TiO_2 depletion is caused by the stabilization of magnetite among the fractionating phase assemblage (Fig. 18). The magnetite contains between 15 and 20 wt.% TiO_2 (Geist et al., 1995). The variation of major elements (including FeO, TiO_2 and SiO_2; Fig. 18) can be explained by fractionation of 11% olivine, 28% augite, 37% plagioclase and 6% magnetite from a basaltic parent liquid at conditions of 0.5 kb and QFM-2 (using MELTS). Both Ni and V decrease substantially once magnetite joins the fractionating assemblage and can be modelled using the partition coefficients of D(Ni) spinel/melt=10 and D(V) spinel/melt=30 (calculated using Eq. (2)). These higher values for D(V) are consistent with results for Ti-bearing spinels (Figs. 8 9 12 and 13) and are also in agreement with high values of D(V) for magnetites determined independently by Leeman et al. (1978).

Finally, Ni, Co and V contents of another basalt to latite sequence at Craters of the Moon, Idaho can be modeled using partition coefficients of D(Ni) spinel/melt=10, D(Co) spinel/melt=5 and D(V) spinel/melt=27 (calculated using Eq. (2)). The values for D(V) spinel/melt are also in agreement with earlier estimates by Leeman et al. (1976) for the same suite.

6. Summary and conclusions

Partitioning of compatible elements (Ni, Co, V) between spinel and silicate melt is thought to be dependent upon many variables: temperature, oxygen fugacity, and spinel composition and structure (Lindstrom, 1976; Horn et al., 1994; Nielsen et al., 1994; Canil, 1997). Our results show that D(Ni) and D(Co) spinel/melt are well constrained and are not particularly sensitive to temperature or oxygen fugacity, but instead to variation in the concentration of Ni and Co, respectively, in spinel. In comparison, D(V) spinel/melt is strongly dependent upon temperature, oxygen fugacity and spinel composition (especially Ti and V content). Future work is needed to unambiguously isolate the role of these variables. For instance, adherence to Henry's Law can be tested best by using a simple system and keeping two of temperature, oxygen fugacity and spinel composition constant, while varying the remaining variable. Similarly, isolation of the effect of spinel composition should strive to keep oxygen fugacity constant, and vice versa. In addition, a better understanding of the valence of V in spinels (e.g., Righter et al., 2005) will help interpretation of partitioning data. Finally, the effect of pressure and melt composition should be investigated.

Acknowledgements

This research is supported by NSF grant EAR-0074036 and a NASA RTOP to Righter. Leeman's efforts on this project were partly supported by NSF Grant EAR-0003612. K. Domanik, C. Schwandt and L. Le assisted with electron microprobe analysis. Discussions with M.J. Drake, J.J. Papike, C.K. Shearer, A. Brandon, J. Jones and C.-T. Lee were useful in understanding these data. Comments on an earlier version of this paper by D. Canil, R. Nielsen, W. van Westrenen and J. van Orman, as well as two anonymous journal reviewers, greatly improved the presentation. **[RR]**

References

Albarède, F., 1996. High-resolution geochemical stratigraphy of Mauna Kea flows from the Hawaii Scientific Drilling Project core. J. Geophys. Res. 101, 11841–11854.

Ariskin, A.A, Barmina, G.S., 1999. An empirical model for the calculation of spinel–melt equilibria in mafic igneous systems at atmospheric pressure: 2. Fe–Ti oxides. Contrib. Mineral. Petrol. 134, 251–263.

Ariskin, A.A, Nikolaev, G.S., 1996. An empirical model for the calculation of spinel–melt equilibria in mafic igneous systems at atmospheric pressure: 1. Chromian spinels. Contrib. Mineral. Petrol. 123, 282–292.

Baker, M.B., Alves, S., Stolper, E., 1996. Petrography and petrology of the Hawaii Scientific Drilling Project lavas: inferences from olivine phenocryst abundances and compositions. J. Geophys. Res. 101, 11715–11728.

Barnes, S.J., 1986. The distribution of chromium among orthopyroxene, spinel, and silicate liquid at atmospheric pressure. Geochim. Cosmochim. Acta 50, 1889–1909.

Borisov, A.A., Kadik, A.A., Zharkova, Ye. V., Kalinichenko, N.V., 1987. Effects of oxygen fugacity on the ratio between valency forms of vanadium in magmas. Geokhimiya 7, 915–920.

Canil, D., 1997. Vanadium partitioning and the oxidation state of Archaean komatiite magmas. Nature 389, 842–845.

Canil, D., 1999. Vanadium partitioning between orthopyroxene, spinel, and silicate melt, and the redox states of mantle source regions for primary magmas. Geochim. Cosmochim. Acta 63, 557–572.

Canil, D., 2002. Vanadium in peridotites, mantle redox and tectonic environments: Archean to present. Earth Planet. Sci. Lett. 195, 75–90.

Capobianco, C.J., Amelin, A., 1994. Metal–silicate partitioning of nickel and cobalt: the influence of temperature and oxygen fugacity. Geochim. Cosmochim. Acta 58, 125–140.

Carmichael, I.S.E., 1967. Iron–titanium oxides and oxygen fugacity in volcanic rocks. J. Geophys. Res. 72, 4665–4687.

Chen, C.-Y., Frey, F.A., Garcia, M.O., 1990. Evolution of alkalic lavas at Haleakala Volcano, East Maui, Hawaii. Contrib. Mineral. Petrol. 105, 197–218.

Christie, D.M., Carmichael, I.S.E., Langmuir, C.H., 1986. Oxidation states of mid-ocean ridge basalt glasses. Earth Planet. Sci. Lett. 79, 397–411.

Delaney, J.S., Sutton, S.R., Newville, M., Jones, J.H., Hanson, B., Dyar, M.D., Schreiber, H.D., 2002. Synchrotron micro-XANES measurements of V oxidation state in glasses as a function of oxygen fugacity: experimental calibration of data relevant to partition coefficient determination. LPSC XXXI, abstract 1806.

Geist, D., Howard, K.A., Larson, P., 1995. The generation of oceanic rhyolites by crystal fractionation: the basalt-rhyolite association at Volcan Alcedo, Galapagos Archipelago. J. Petrol. 36, 965–982.

Ghiorso, M.S., Sack, R.O., 1994. Chemical mass transfer in magmatic processes: IV. A revised an internally consistent thermodynamic model for the interpolation and extrapolation of liquid–solid equilibria in magmatic systems at elevated temperatures and pressures. Contrib. Mineral. Petrol. 119, 197–212.

Green, T.H., 1994. Experimental studies of trace element partitioning applicable to igneous petrogenesis—Sedona 16 years later. Chem. Geol. 117, 1–36.

Hanson, B., Jones, J.H., 1998. The systematics of Cr^{3+} and Cr^{2+} partitioning between olivine and liquid in the presence of spinel. Am. Mineral. 83, 669–684.

Hill, R.J., Craig, J.R., Gibbs, G.V., 1979. Systematics of the spinel structure type. Phys. Chem. Mineral. 4, 317–339.

Holzheid, A., Palme, H., 1996. The influence of FeO in the solubilities of Co and Ni in silicate melts. Geochim. Cosmochim. Acta 60, 1181–1193.

Horn, I., Foley, S.F., Jackson, S.E., Jenner, G.A., 1994. Experimentally determined partitioning of high field strength and selected transition elements between spinel and basaltic melt. Chem. Geol. 117, 193–218.

Irving, A.J., 1978. A review of experimental studies of crystal/liquid trace element partitioning. Geochim. Cosmochim. Acta 42, 743–770.

Kress, V.C., Carmichael, I.S.E., 1991. The compressibility of silicate liquids containing Fe_2O_3 and the effect of composition, temperature, oxygen fugacity and pressure on their redox states. Contrib. Mineral. Petrol. 108, 82–92.

Leeman, W.P., 1974. Experimental determination of the partitioning of divalent cations between olivine and basaltic liquid, Pt. II. PhD Thesis, Univ. Oregon, 231–337.

Leeman, W.P., Lindstrom, D.J., 1978. Partitioning of Ni^{2+} between basaltic and synthetic melts and olivine—an experimental study. Geochim. Cosmochim. Acta 42, 800–816.

Leeman, W.P., Vitaliano, C.J., Prinz, M., 1976. Evolved lavas from the Snake River Plain: Craters of the Moon National Monument, Idaho. Contrib. Mineral. Petrol. 56, 35–60.

Leeman, W.P., Ma, M.-S., Murali, A.V., Schmitt, R.A., 1978. Empirical estimation of magnetite/liquid distribution coefficients from some transition elements. Contrib. Mineral. Petrol. 65, 269–272.

Lindstrom, D.J., 1976. Experimental study of the partitioning of the transition metals between clinopyroxene and coexisting silicate liquids. Univ. Oregon, PhD Thesis.

Maurel, C., Maurel, P., 1983. Étude expérimentale de l'équilibre Fe^{2+}–Fe^{3+} dans les spinelles chromifères et les liquides silicatés basiques coexistants, à 1 atm. C. R. Acad. Sci. 295, 209–212.

Myers, J., Eugster, H., 1983. The system Fe–Si–O: oxygen buffer calibrations to 1500 K. Contrib. Mineral. Petrol. 82, 75–85.

Mysen, B.O., 1991. Relations between structure, redox equilibria of iron, and properties of magmatic liquids. In: Perchuk, L.L., Kushiro, I. (Eds.), Physical Chemistry of Magmas. Springer-Verlag, New York.

Nehru, C.E., Prinz, M., Dowty, E., Keil, K., 1974. Spinel-group minerals and ilmenite in Apollo 15 rake samples. Am. Mineral. 59, 1220–1235.

Nielsen, R.L., Forsythe, L.M., Gallahan, W.E., Fisk, M.R., 1994. Major- and trace-element magnetite–melt equilibria. Chem. Geol. 117, 167–191.

O'Neill, H.St.C., 1987. Quartz–fayalite–iron and quartz–fayalite–magnetite equilibria and the free energy of formation of fayalite and magnetite. Am. Mineral. 72, 67–75.

O'Neill, H.St.C., Pownceby, M.I., 1993a. Thermodynamic data from redox reactions at high temperatures: II. The MnO–Mn_3O_4 oxygen buffer and implications for the thermodynamic properties of MnO and Mn_3O_4. Contrib. Mineral. Petrol. 114, 315–320.

O'Neill, H.St.C., Pownceby, M.I., 1993b. Thermodynamic data from redox reactions at high temperatures: I. An experimental and theoretical assessment of the electrochemical method using stabilized zirconia electrolytes, with revised values for the Fe–"FeO", Co–CoO, Ni–NiO and Cu–Cu_2O oxygen buffers, and new data for the W–WO_2 buffer. Contrib. Mineral. Petrol. 114, 296–314.

Papike, J.J., Karner, J.M., Shearer, C.K., 2005. Comparative planetary mineralogy: valence state partitioning of Cr, Fe, Ti and V among crystallographic sites in olivine, pyroxene, and spinel from planetary basalts. Am. Mineral. 90, 277–290.

Pownceby, M.I., O'Neill, H.St.C., 1994. Thermodynamic data from redox reactions at high temperatures: IV. Calibration of the Re–ReO_2 oxygen buffer from EMF and NiO+Ni–Pd redox sensor measurements. Contrib. Mineral. Petrol. 118, 130–137.

Pouchou, J.-L., Pichoir, F., 1991. Quantitative analysis of homogeneous or stratified microvolumes applying the model "PAP". In: Heinrich, K.F.J., Newbury, D.E. (Eds.), Electron Microprobe Quantitation. Plenum Press, New York, pp. 31–75.

Puchtel, I., Humayun, M., 2000. Platinum group elements in Kostomuksha komatiites and basalts: implications for oceanic crust

recycling and core–mantle interaction. Geochim. Cosmochim. Acta 64, 4227–4242.

Puchtel, I.S., Brügmann, Hofmann, A.W., 1998. Precise Re–Os mineral isochron and Pb–Nd–Os isotope systematics of a mafic–ultramafic sill in the 2.0 Ga Onega plateau (Baltic Shield). Earth Planet. Sci. Lett. 170, 447–461.

Rhodes, J.M., 1996. Geochemical stratigraphy of lava flows sampled by the Hawaii Scientific Drilling Project. J. Geophys. Res. 101, 11729–11746.

Righter, K., Drake, M.J., Yaxley, G., 1997. Prediction of siderophile element metal–silicate partition coefficients to 20 GPa and 2800 °C: the effect of pressure, temperature, fO_2 and silicate and metallic melt composition. Phys. Earth Planet. Int. 100, 115–134.

Righter, K., Campbell, A.J., Humayun, M., 2004. Partitioning of Re, Ir, Rh, and Ru between Cr-bearing spinel and silicate melts. Geochim. Cosmochim. Acta 68, 867–880.

Righter, K., Sutton, S.R., Newville, M., Le, L., Schwandt, C., 2005. Micro-XANES measurements on experimental spinels and the oxidation state of vanadium in coexisting spinel and silicate melt. Lunar Planet. Sci. (XXXVI, #1140).

Roeder, P.L., Reynolds, I., 1991. Crystallization of chromite and chromium solubility in basaltic melts. J. Petrol. 32, 909–934.

Schilling, J.-G., Zajac, M., Evans, R., Johnston, T., White, W., Devine, J.D., Kingsley, R., 1983. Petrologic and geochemical variations along the mid-Atlantic Ridge from 29° to 73°N. Am. J. Sci. 283, 510–586.

Schreiber, H.D., Merkel, R.C., Schreiber, L.V., Balazs, G.B., 1987. Mutual interactions of redox couples via electron exchange in silicate melts: models for geochemical systems. J. Geophys. Res. 92, 9233–9245.

Shimizu, N., Semet, M.P., Allegre, C.J., 1978. Geochemical applications of quantitative ion microprobe analysis. Geochim. Cosmochim. Acta 42, 1321–1334.

Snyder, D.A., Carmichael, I.S.E., 1992. Olivine–liquid equilibria and the chemical activities of FeO, NiO, Fe_2O_3, and MgO in natural basic melts. Geochim. Cosmochim. Acta 56, 303–318.

Steele, I.M., Lindstrom, D.J., 1981. Ni partitioning between diopside and silicate melt: a redetermination by ion microprobe and recognition of experimental complication. Geochim. Cosmochim. Acta 45, 2177–2183.

Steele, I.M., Hervig, R.L., Hutcheon, I.D., Smith, J.V., 1981. Ion microprobe techniques and analyses of olivine and low Ca-pyroxene. Am. Mineral. 66, 526–546.

Toplis, M.J., Corgne, A., 2002. An experimental study of element partitioning between magnetite, clinopyroxene and iron-bearing silicate liquids with particular emphasis on vanadium. Contrib. Mineral. Petrol. 144, 22–37.

Waychunas, G.A., 1991. Crystal chemistry of oxides and oxyhydroxides. In: Lindsley, D.H. (Ed.), Oxide Minerals: Petrologic and Magnetic Significance, Rev. Mineral., vol. 25. Mineral. Soc. Amer., Washington, DC, pp. 11–68.